

**FRMD8 promotes inflammatory and growth factor signalling by stabilising the
iRhom/ADAM17 sheddase complex**

Ulrike Künzel, Adam G. Grieve, Yao Meng², Boris Sieber, Sally A. Cowley, Matthew
Freeman*

Sir William Dunn School of Pathology

University of Oxford

South Parks Road

Oxford OX1 3RE

² Current address:

Department of Biochemistry

University of Oxford

South Parks Road

Oxford OX1 3QU

*Correspondence to Lead Contact: matthew.freeman@path.ox.ac.uk

Abstract

Many intercellular signals are synthesised as transmembrane precursors that are released by proteolytic cleavage ('shedding') from the cell surface. ADAM17, a membrane-tethered metalloprotease, is the primary shedding enzyme responsible for the release of the inflammatory cytokine TNF α and several EGF receptor ligands. ADAM17 exists in complex with the rhomboid-like iRhom proteins, which act as cofactors that regulate ADAM17 substrate shedding. Here we report that the poorly characterised FERM domain-containing protein FRMD8 is a new component of iRhom2/ADAM17 sheddase complex. FRMD8 binds to the cytoplasmic N-terminus of iRhoms and is necessary to stabilise the iRhoms and ADAM17 at the cell surface. In the absence of FRMD8, iRhom2 and ADAM17 are degraded via the endolysosomal pathway, resulting in the reduction of ADAM17-mediated shedding. We have confirmed the pathophysiological significance of FRMD8 in iPSC-derived human macrophages and mouse tissues, thus demonstrating its role in the regulated release of multiple cytokine and growth factor signals.

Introduction

The cell surface protease ADAM17 (also called TACE) mediates the release of many important signalling molecules by 'shedding' their extracellular ligand domains from transmembrane precursors. A prominent example is the role of ADAM17 in releasing the tumour necrosis factor alpha (TNF α) (Black et al., 1997, Moss et al., 1997), a primary cytokine involved in the inflammatory responses to infection and tissue damage (Kalliolias and Ivashkiv, 2016). In addition, ADAM17 is the principal sheddase of the epidermal growth factor (EGF) receptor ligands amphiregulin (AREG), transforming growth factor alpha (TGF α), heparin-binding EGF (HB-EGF), epigen, and epiregulin (Sahin et al., 2004, Sahin and Blobel, 2007). The control of ADAM17 activity has therefore been the focus of much fundamental and pharmaceutical research (reviewed in (Rose-John, 2013, Zunke and Rose-John, 2017)). We and others have previously reported that the rhomboid-like iRhom proteins have a specific and extensive regulatory relationship with ADAM17, to the extent that iRhoms can effectively be considered as regulatory subunits of the protease (Grieve et al., 2017). iRhoms are members of a wider family of evolutionarily related multi-pass membrane proteins, called the rhomboid-like superfamily (Freeman, 2014). The family is named after the rhomboids, intramembrane serine proteases that cleave substrate transmembrane domains (TMDs), but many members, including iRhoms, have lost protease activity during evolution.

iRhom1 and its paralogue iRhom2 (encoded by the genes *RHBDF1* and *RHBDF2*) show redundancy in regulating ADAM17 maturation, but differ in their tissue expression (Christova et al., 2013). Many cell types express both iRhoms, so the loss of one can be compensated by the other (Christova et al., 2013, Li et al., 2015). Macrophages are, however, an exception: iRhom1 is not expressed, so iRhom2 alone regulates ADAM17 and therefore TNF α inflammatory signalling in macrophages (Adrain et al., 2012, McIlwain et al., 2012, Issuree et al., 2013). iRhoms control ADAM17 activity in multiple ways. First, they bind to the catalytically immature pro-form of ADAM17 (proADAM17) in the endoplasmic reticulum (ER), and are required for its trafficking from the ER to the Golgi apparatus (Adrain et al., 2012, McIlwain et al., 2012). Once proADAM17 reaches the Golgi, it is matured by the removal of its inhibitory pro-domain by pro-protein convertases (Schlondorff et al., 2000, Endres et al., 2003) and is further trafficked to the plasma membrane. iRhoms have further regulatory functions beyond this step of ADAM17 maturation. Still bound to each other, iRhom2 prevents the lysosomal degradation of ADAM17 (Grieve et al., 2017). Later, iRhom2 controls the activation of ADAM17: phosphorylation of the iRhom2 cytoplasmic tail promotes the recruitment of 14-3-3 proteins, which promote shedding activity of ADAM17, thereby releasing TNF α from the cell surface in response to inflammatory triggers (Grieve et al., 2017, Cavadas et al., 2017). Finally, iRhoms are also reported to contribute to ADAM17 substrate specificity (Issuree et al., 2013). This intimate regulatory role of iRhoms make them essential players in ADAM17-mediated signalling and thus new targets for manipulating inflammatory signalling. The significance of this potential is underlined by the fact that anti-TNF α therapies, used to treat rheumatoid arthritis and other inflammatory diseases, are currently the biggest grossing drugs in the world (Monaco et al., 2015).

Despite the role of the iRhom/ADAM17 shedding complex in controlling signalling, much is yet to be understood about the molecular mechanisms that control this inflammatory trigger. To identify the wider machinery by which iRhoms regulate ADAM17, we report here a proteomic screen to identify their binding partners. We have identified the poorly characterised FERM domain-containing protein 8 (FRMD8) as having a strong and specific interaction with the cytoplasmic N-terminus of iRhoms. The functional significance of this interaction is demonstrated by loss of FRMD8 causing a similar phenotype to iRhom deficiency in cells: loss of mature ADAM17 and severely reduced shedding of ADAM17 substrates from the cell surface. We show that loss of FRMD8 leads to lysosomal degradation of mature ADAM17 and iRhom2, indicating that its function is to stabilise the iRhom/ADAM17 sheddase complex once it reaches the plasma membrane. Overall, our results imply that FRMD8 is an essential component of the inflammatory signalling machinery. To test this proposal *in vivo* we deleted the *FRMD8* gene in human induced pluripotent stem cells (iPSCs) and differentiated them into macrophages. Consistent with our

biochemical data, these mutant macrophages were defective in their ability to release TNF α in response to lipopolysaccharide (LPS) stimulation, demonstrating the pathophysiological importance of FRMD8 in the normal inflammatory response by human macrophages. The *in vivo* significance of FRMD8 in regulating the stability of the iRhom/ADAM17 shedding complex was further reinforced by our observation that mature ADAM17 and iRhom2 protein levels are strongly reduced in tissues of FRMD8-deficient mice.

Results

FRMD8 is a novel interaction partner of iRhom1 and iRhom2

To investigate the molecular mechanisms that underlie iRhom2 functions, we performed a mass spectrometry-based screen to identify new proteins that interact with human iRhom2. iRhom2-3xHA was stably expressed in human embryonic kidney (HEK) 293T cells and immunoprecipitated. The bead eluates containing immunoprecipitated iRhom2 and its interacting proteins were analysed by label-free mass spectrometry. As a negative control, we did the same analysis in parallel with 3xHA-tagged UNC93B1, an unrelated polytopic protein that, like iRhom2, is predominantly located in the ER (Koehn et al., 2007) (Figure 1-figure supplement 1A). Quantitative protein abundance data from three biological replicates of Rhom2 and UNC93B1 co-immunoprecipitations were statistically analysed using the Perseus software platform (Tyanova et al., 2016). Validating the overall approach, we detected ADAM17, the known iRhom2 interacting protein (Adrain et al., 2012, McIlwain et al., 2012, Christova et al., 2013) as a statistically significant hit (Figure 1A, Table1). Among the hits were several 14-3-3 proteins (eta, epsilon, gamma, sigma, theta, zeta/delta) and MAPK1/3 (Table 1), which we have previously reported to participate in the regulation of inflammatory signalling by phosphorylation of iRhom2 (Grieve et al., 2017). The top hit by a long way, however, was FRMD8 (Figure 1A, Table 1), a poorly studied protein that has not previously been implicated in iRhom function, ADAM17 regulation, and growth factor or cytokine signalling.

We confirmed the interaction between iRhom2 and FRMD8 by immunoprecipitation. C-terminally V5-tagged FRMD8 co-immunoprecipitated with either iRhom1-3xHA or iRhom2-3xHA (Figure 1B). Conversely, we pulled down both iRhom1-3xHA and iRhom2-3xHA with an antibody against the V5 tag. Finally, we were also able to co-immunoprecipitate endogenous FRMD8 with iRhom2-3xHA (Figure 1-figure supplement 1B). Together these results identify FRMD8 as a bona fide binding partner of iRhom1 and iRhom2 in human cells.

FRMD8 is required for iRhom function

As its name indicates, FRMD8 is a FERM (4.1/ezrin/radixin/moesin) domain-containing protein. It is predicted to be a soluble cytoplasmic protein, and the only report about its function describes it as binding to the Wnt accessory receptor low-density lipoprotein receptor-related protein 6 (LRP6), and negatively regulating Wnt signalling (Kategaya et al., 2009). To investigate the functional significance of FRMD8 binding to iRhoms, we examined the effects of loss of FRMD8 on iRhom function in HEK293T cells, using both siRNA and CRISPR/Cas9-mediated gene deletion (Figure 2A, B). In both cases, loss of FRMD8 drastically reduced the protein levels of mature ADAM17 (Figure 2A, B). This effect was specific to ADAM17, as the maturation of its closest homologue, ADAM10, was unaffected by loss of FRMD8 (Figure 2B). Moreover, mature ADAM17 levels were rescued by expression of FRMD8-V5 in FRMD8 knockout HEK293T cells (Figure 2C), confirming that the phenotype was caused by FRMD8 loss. Finally, in addition to this reduction of mature ADAM17 caused by FRMD8 loss, we found a striking loss of ADAM17, but not ADAM10, on the cell surface (Figure 2D). These phenotypes partially phenocopy the loss of iRhoms (Christova et al., 2013, Grieve et al., 2017), consistent with FRMD8 being needed for iRhoms to act as positive regulators of ADAM17.

We also examined the consequences of loss of FRMD8 on ADAM17-dependent signalling. The shedding of alkaline phosphatase (AP)-tagged EGF receptor ligands AREG and HB-EGF, after stimulation with phorbol 12-myristate 13-acetate (PMA), were both substantially reduced in FRMD8 knockout cells (Figure 2E). To exclude the possibility that the defect in FRMD8 knockout cells is an inability to respond to PMA, we measured both PMA-stimulated and unstimulated, constitutive shedding of AP-tagged TGF α , another major EGFR ligand. Again, FRMD8 knockout cells released significantly less AP-TGF α compared to wild-type cells, both after stimulation but also after 20 h of constitutive shedding (Figure 2F), implying that mutant cells had fundamental defects in their ability to shed ADAM17 ligands, regardless of PMA stimulation. To demonstrate that the release of ligands was indeed caused by metalloprotease shedding and not simply an indication of leakage caused by cell death, we showed that it was sensitive to the ADAM10/17 inhibitor GW280264X (GW) (Figure 2E, F). Overall, as with ADAM17 maturation, the shedding defects in FRMD8-deficient cells resemble those caused by the loss of iRhoms.

FRMD8 binds to the cytoplasmic iRhom2 N-terminus and regulates mature ADAM17 levels

As described above, iRhoms regulate ADAM17 function at multiple stages: from ER-to-Golgi trafficking, to the activation of the sheddase at the cell surface. To address where FRMD8 fits in this long-term relationship between iRhoms and ADAM17, we started by analysing the FRMD8 binding site within iRhom2. As a cytoplasmic protein, FRMD8 was

likely to bind to the only substantial cytoplasmic region of iRhom2, its N-terminus. We therefore made a set of iRhom2-3xHA N-terminal deletion constructs (Figure 3A) to locate the binding site. Deletion of the first 200 amino acids in the N-terminus of iRhom2 (iRhom2^{Δ200}) did not disrupt FRMD8 binding, but no interaction was detected in mutants greater than Δ300 (Figure 3B), implying that the region between 200 and 300 amino acids was necessary for FRMD8 binding. An internal deletion of amino acids 201-300 within iRhom2 (iRhom2^{Δ201-300}) led to the loss of exogenous FRMD8 binding (Figure 3C), confirming that the FRMD8 binding site lies within this region. In line with this, an iRhom1/2 DKO cell line reconstituted with iRhom2^{Δ201-300} showed a similar deficiency to FRMD8 KO cells in ADAM17-mediated shedding of AREG (compare Figure 3D and 2E). This reduction in shedding correlates with a reduction in the level of mature ADAM17 (Figure 3E). Overall, this makes the iRhom2^{Δ201-300} mutant a useful tool to study the loss of FRMD8 binding to iRhom2 and highlights that FRMD8 binding affects levels of mature ADAM17, presumably either through controlling ADAM17 maturation or stability. Interestingly, the FRMD8 binding site is also absent in a mouse iRhom2 mutant called *curly-bare (cub)*, which lacks residues 1-268 (Hosur et al., 2014, Siggs et al., 2014). Sequence alignment shows that the deletion of 268 amino acids in mouse iRhom2 corresponds to the loss of residues 1-298 in the human protein (Figure 3-figure supplement 1A). Consistent with this mapping data, we found that whereas full-length mouse iRhom2 bound human FRMD8, the *cub* mutant cannot (Figure 3-figure supplement 1B). This failure of FRMD8 binding presumably contributes to the complex defects that underlie the *cub* phenotype (Johnson et al., 2003, Hosur et al., 2014, Siggs et al., 2014).

Combined, these data show that FRMD8 is recruited to a discrete 201-300 amino acid region of the iRhom2 N-terminus, and that this binding is required for sufficient levels of mature ADAM17, as well as ADAM17-dependent shedding.

FRMD8, iRhom2, and ADAM17 form a tripartite complex

We next investigated the nature of a putative tripartite complex between iRhom2, FRMD8 and ADAM17. Previous work has shown a strong interaction between iRhom2 and ADAM17 (Adrain et al., 2012, McIlwain et al., 2012, Grieve et al., 2017), yet how FRMD8 intersects with this complex is not known. When performing an immunoprecipitation of FRMD8, we found both immature and mature ADAM17 as well as iRhom2 (Figure 4A). This indicates that FRMD8 does indeed form a tripartite complex with ADAM17 and iRhom2. To test this further, we performed a series of pairwise co-immunoprecipitations in the absence of FRMD8, ADAM17 or iRhoms. First we tested the requirement for ADAM17 in the iRhom2/FRMD8 interaction. We found that exogenous FRMD8 and iRhom2 co-immunoprecipitated with each other in ADAM17 knockout cells (Figure 4B). In turn, iRhom2

and ADAM17 were still able to interact with each other in FRMD8 knockout cells (Figure 4C), showing that FRMD8 is not essential for the iRhom/ADAM17 sheddase complex to form. In contrast, FRMD8 did not pull down ADAM17 in cells mutant for both iRhoms (Figure 4D). This demonstrated that there is no direct link between FRMD8 and ADAM17; instead both bind simultaneously to iRhom2. Supporting this, FRMD8 co-immunoprecipitated with pro- or mature ADAM17 in iRhom1/2 DKO cells reconstituted with iRhom2^{WT}, but not with iRhom2^{Δ201-300} (Figure 4D), the mutant that does not bind to FRMD8 (Figure 3C). FRMD8 binds to both iRhom2/proADAM17 and iRhom2/mature ADAM17 complexes but associates preferentially with iRhom2/mature ADAM17 complexes (Figure 4A, D), which have been shown to exist at the cell surface (Grieve et al., 2017, Cavadas et al., 2017). This is consistent with the observation of specific effects of FRMD8 loss on mature ADAM17 at the cell surface, but not immature ADAM17 (Figure 2A-C).

FRMD8 recruitment promotes cell surface localisation of iRhom2 and ADAM17

To further investigate a potential role for FRMD8 at the cell surface, we first assessed its effects on iRhom2 localisation by immunofluorescence. Overexpression of FRMD8-V5 in iRhom1/2 DKO cells reconstituted with wild-type iRhom2 led to a striking increase in plasma membrane iRhom2 (Figure 5A), which in wild-type cells is almost exclusively observed within the endoplasmic reticulum (Figure 1-figure supplement 1A). As a control, the iRhom2^{Δ300} mutant, which cannot bind to FRMD8 (Figure 3B), did not undergo the same ER-to-plasma membrane relocalisation upon FRMD8 overexpression. Indicating a reciprocal relationship between the two proteins, we also observed that the iRhom2 N-terminus was required for FRMD8 localisation at the cell surface (Figure 5A, B).

To test whether FRMD8 is sufficient to target iRhom2 to the cell surface, we fused FRMD8 to the N-terminus of the ER-localised iRhom2^{Δ300} mutant (FRMD8-iRhom2^{Δ300}). Strikingly, we saw that the normal ER localisation of iRhom2^{Δ300} (Figure 5D) shifted to the plasma membrane upon fusion to FRMD8 (Figure 5E). Furthermore, we found that the localisation of ADAM17-V5 followed that of iRhom in both conditions: in iRhom2^{Δ300} cells ADAM17 localised to the ER, and in FRMD8-iRhom2^{Δ300} cells it was readily observed at the cell surface. We also noted that FRMD8-iRhom2^{Δ300} showed strikingly higher total levels of iRhom2 (Figure 5E), which hinted that FRMD8 may play a role in the protein turnover of iRhoms at the cell surface. In line with these observations, we found that FRMD8-iRhom2^{Δ300} was much more stable compared to iRhom2^{Δ300} or iRhom2 WT as seen in cells incubated with cycloheximide (CHX) to block the synthesis of new proteins (Figure 5F). Taken together, these data suggest that FRMD8 binding to iRhom2 stabilises the iRhom2 pool in the late secretory pathway and increases the cell surface localisation of the iRhom2/ADAM17 sheddase complex.

FRMD8 recruitment protects iRhom2/ADAM17 from lysosomal degradation

Previous studies have shown that the cytoplasmic N-terminal region of iRhom2 is required to prevent lysosomal degradation of ADAM17 (Grieve et al., 2017). Therefore, we questioned whether the absence of FRMD8 recruitment to the iRhom2 N-terminus led to delivery of iRhom and ADAM17 to lysosomes. By immunofluorescence microscopy, iRhom2^{WT} localisation is indistinguishable from iRhom2^{Δ300} (Figure 6A, B) within the endoplasmic reticulum (Figure 1-figure supplement 1A). However, upon treatment with the lysosomal degradation inhibitor, bafilomycin A1, both proteins accumulated in LAMP1-positive lysosomal puncta (Figure 6C, D). This suggests that there is a constant turnover of iRhom2 through the endo-lysosomal pathway, with iRhoms presumably cycling via the plasma membrane, before being degraded. Interestingly, unlike the partial colocalisation between LAMP1 and iRhom2^{WT} (Figure 6C), iRhom2^{Δ300} overlapped completely with LAMP1 (indicated by the arrows in Figure 6D). This confirmed that in the absence of FRMD8 recruitment, iRhom2 is constitutively sent to lysosomes. Importantly, this lysosomal pool of iRhom2^{Δ300} also colocalised with ADAM17-V5 after bafilomycin treatment (highlighted with arrows in Figure 6F). All these data together indicate that the iRhom2/ADAM17 complex follow the same fate in the absence of FRMD8 recruitment (Figure 6E, F). Using a complementary approach, we tested the stability of ADAM17 in FRMD8 knockout cells. After 16 h of treatment with the lysosomal degradation inhibitors bafilomycin and ammonium chloride, the mature form of ADAM17 was partially restored (Figure 6G; Figure 7-figure supplement 1B).

Combined, these results explain the reduced level of mature ADAM17 in FRMD8 knockout cells: it implies that the defect caused by loss of FRMD8 is not a failure of ADAM17 maturation, but instead a failure to stabilise the mature form. In line with this interpretation, the proteasomal inhibitor MG132 had no effect on the stability of mature ADAM17 (Figure 7A). We conclude that FRMD8 binding to iRhom2 acts to promote ADAM17 function by ensuring its stability after its maturation in the *trans*-Golgi network.

FRMD8 functions to stabilise levels of iRhoms at the cell surface

If FRMD8 acts as a stabilising factor for the plasma membrane-localised iRhom2/ADAM17 sheddase complex, a difference in the cell surface level of iRhom2 is expected in the absence of FRMD8. Most tagged iRhom2 is ER-localised (Figure 1-figure supplement 1A, Figure 6A) and the cell surface fraction is relatively small (Maney et al., 2015, Grieve et al., 2017). Therefore, we used cell surface immunostaining of iRhom2 followed by flow cytometry to measure specifically the pool of iRhom2 at the cell surface. In the absence of FRMD8 we detected a significant loss of cell surface iRhom2 (Figure 7A). In

line with our observation that cell surface iRhom2 represents only a small fraction of the total pool, a reduction of total iRhom2 levels was not detectable (Figure 7B). This further supports our observations that FRMD8 binding to iRhoms is required to stabilise the cell surface pool of iRhoms. Consistent with our conclusion that FRMD8 primarily functions late in the iRhom2/ADAM17 relationship, we detected no defects in the ER iRhom2/proADAM17 interaction in FRMD8 knockout cells (Figure 4C), nor in the trafficking of iRhom2 from the ER to the Golgi (Figure 7-figure supplement 1C).

These results show that by binding to iRhom2, FRMD8 stabilises both iRhom2 and mature ADAM17, protecting them from degradation. A more direct demonstration of this stabilising function is provided by overexpressing FRMD8, which leads to increased levels of tagged iRhom2 (Figure 7C), as well as iRhom1 (Figure 7-figure supplement 1D). Note that the 50 kDa N-terminally truncated fragment of iRhoms detected in western blots (Nakagawa et al., 2005, Adrain et al., 2012, Maney et al., 2015) is not stabilised by FRMD8 expression (Figure 7C, Figure 7-figure supplement 1D). This iRhom fragment lacks the cytoplasmic tail, and therefore the binding site for FRMD8, so its insensitivity to FRMD8 is consistent with our model. Intriguingly, the stabilisation of iRhom2 and FRMD8 is mutual: overexpression of iRhom2 consistently led to the stabilisation of endogenous FRMD8 protein (Figure 7D) without affecting FRMD8 mRNA levels (Figure 7E). This indicates that the iRhom2-FRMD8 interaction leads to mutual stabilisation of both proteins and as well as mutual effects on plasma membrane localisation (Figure 5A).

To ensure that our conclusion that FRMD8 stabilises iRhoms was not distorted by our use of overexpressed proteins, and in the absence of a usable antibody against human iRhom2, we used CRISPR/Cas9 to insert a triple HA tag into the *RHBDF2* locus to express endogenously C-terminally tagged iRhom2. siRNA-mediated knockdown of iRhom2 confirmed that this editing was successful (Figure 8A). The cells showed no defect in ADAM17 maturation (Figure 8A, Figure 7-figure supplement 1E), indicating that the tagged protein was functional. In these cells FRMD8 overexpression led to an increase in endogenous iRhom2 levels (Figure 8A); conversely, siRNA knockdown of FRMD8 caused a reduction of iRhom2 protein (Figure 8B), but no change of iRhom2 mRNA levels (Figure 8C). Again, the 50 kDa iRhom2 fragment was not affected by FRMD8 levels (Figure 8A, B). Parenthetically, this is the first reported evidence that this iRhom fragment exists endogenously, although its functional significance remains unclear.

To summarise our results to this point, we have discovered that by binding to the iRhom2 cytoplasmic N-terminus, FRMD8 stabilises the cell surface iRhom2/ADAM17 sheddase complex. In the absence of FRMD8 recruitment to iRhom2, this enzyme complex is sent to lysosomes and degraded.

FRMD8 binding to iRhom2 is essential for inflammatory signalling in human macrophages

We tested the pathophysiological significance of our conclusions by analysing the consequence of loss of FRMD8 in human macrophages, which release TNF α in response to tissue damage and inflammatory stimuli. To generate mutant human macrophages, we used CRISPR/Cas9 to knock out FRMD8 in an iPSC line that had previously been generated from dermal fibroblasts of a healthy female donor (Fernandes et al., 2016). The FRMD8 knockout and control iPSCs were analysed for deletions in the *FRMD8* gene by PCR (Figure 9-figure supplement 1A), and a normal karyotype was confirmed by single nucleotide polymorphism (SNP) analysis (Figure 9-figure supplement 1B) before differentiation into macrophages (Figure 9A). These mutant macrophages expressed no detectable FRMD8 and, as in the HEK293T cells, showed severely reduced levels of mature ADAM17 (Figure 9B). When challenged with the inflammatory trigger LPS, TNF α shedding from the cells, as measured by ELISA, was reduced (Figure 9C). Confirming the expected specificity, the ADAM10 inhibitor GI254023X (GI) had no effect on TNF α release from these cells, whereas GW, an inhibitor of both ADAM10 and ADAM17, further reduced TNF α release (Figure 9-figure supplement 1C). Although shedding was inhibited, TNF α expression by LPS was normal in these cells (Figure 9-figure supplement 1D). These results demonstrate that our conclusions about the requirement for FRMD8 in ADAM17 function in cell culture models does indeed apply to human macrophages.

Loss of FRMD8 in mice highlights its physiological role in stabilising the iRhom/ADAM17 complex

To investigate further the physiological significance of our discovery of the role of FRMD8 in stabilising iRhom/ADAM17 sheddase complexes, we analysed the levels of ADAM17 and iRhom2 in tissues from FRMD8-deficient mice. These mice were generated from embryonic stem (ES) cells from the KOMP Repository, University of California Davis, in which all coding exons (2-11) of the *Frmd8* gene were deleted (Figure 9-figure supplement 2A). *Frmd8*^{-/-} mice are viable (Figure 9-figure supplement 2B) and fertile. The knockout was confirmed by western blot (Figure 9D). Western blot analysis of tissues of *Frmd8*^{-/-} mice showed that mature ADAM17 levels were reduced in all tissues examined compared to tissues from wild-type littermates (Figure 9D). This confirms that FRMD8 controls the level of mature ADAM17 *in vivo*. Of note, there was a major reduction of mature ADAM17 levels in the brain, a tissue in which iRhom2 is almost completely absent but iRhom1 levels are high (Christova et al., 2013, Li et al., 2015). This supports our hypothesis that FRMD8 regulates mature ADAM17 levels through iRhom1 as well as iRhom2. We also tested *in vivo* our conclusion that FRMD8 loss destabilises endogenous iRhoms (Figure 8B). Using an

antibody that we had previously generated against mouse iRhom2 (Adrain et al., 2012), we analysed iRhom2 levels in *Frmd8*^{+/+} and *Frmd8*^{-/-} mouse tissues. In lung and skin, both tissues with high iRhom2 expression (Christova et al., 2013), we detected a strong decrease of iRhom2 protein levels in *Frmd8*^{-/-} compared to wild-type (Figure 9E, Figure 9-figure supplement 2C). Tissue from *Rhbdf2*^{-/-} mice served as a control for the iRhom2 antibody specificity (Figure 9E, Figure 9- figure supplement 2C). The reduction of endogenous iRhom2 and mature ADAM17 levels in mouse lung was about 75% (Figure 9E) which is comparable to the reduction of mature ADAM17 levels in iPSC-derived human macrophages (Figure 9B). In summary, our experiments in mice confirm the physiological importance of our prior conclusions: FRMD8 is required *in vivo* to regulate the stability of the iRhom/ADAM17 sheddase complex and is therefore a previously unrecognised essential component in regulating cytokine and growth factor signalling.

Discussion

ADAM17 is the shedding enzyme that is responsible for not only the activation of inflammatory TNF α signalling, but also the release from the cell surface of multiple EGF family growth factors, and other proteins. Its regulation has therefore received much attention, both from the perspective of fundamental cell biology and because of the proven therapeutic significance of blocking TNF α (Monaco et al., 2015). Here we report that FRMD8 is a new component of the regulatory machinery that controls the release of ADAM17 substrates, including TNF α . We identified FRMD8 as a prominent binding partner of iRhoms, which are rhomboid-like proteins that act as regulatory cofactors of ADAM17. Our subsequent experiments demonstrate that although FRMD8 binds to iRhoms throughout their life cycle, its function appears to be confined to the later stages of their role in regulating ADAM17. FRMD8 stabilises the iRhom2/ADAM17 complex at the cell surface, ensuring it is available to shed TNF α and growth factors. We took advantage of iPSC technology to generate human FRMD8 knockout macrophages, allowing us to confirm that the mechanistic conclusions derived mostly from HEK293T cell models were indeed relevant to the human cells that provide the primary inflammatory response. Finally, tissues from FRMD8 knockout mice demonstrate the physiological importance of FRMD8 in a whole organism, and confirm that it stabilises the iRhom/mature ADAM17 complex *in vivo*.

Bringing together all our results, we propose the following model of FRMD8 function in ADAM17-dependent signalling: FRMD8 binds to the cytoplasmic domain of iRhoms throughout the secretory pathway, forming a tripartite complex when iRhoms are also bound to ADAM17. Despite this long-term relationship, we have found no evidence for a functional

role for FRMD8 in ER-to-Golgi trafficking or ADAM17 maturation. Instead, FRMD8 acts later, to prevent the endolysosomal degradation of the iRhom/ADAM17 complex (Figure 10). The exact molecular detail of FRMD8 action on the iRhom2/ADAM17 sheddase complex is unclear. It is possible that FRMD8 increases the delivery of the iRhom2/ADAM17 sheddase complex from the Golgi apparatus to the cell surface, stabilises the complex by preventing its internalisation, or promotes the endosomal retrieval to the cell surface. In all cases, it is likely that the recruitment of additional proteins is required. Therefore understanding the molecular interactions of FRMD8, as well as the FRMD8/iRhom2/mature ADAM17 complex at the cell surface, will shed light into the molecular mechanism.

As we have previously reported, it is the iRhom2/ADAM17 complex that is responsible for shedding ADAM17 substrates including TNF α . Without FRMD8, iRhoms and mature ADAM17 are destabilised and the cell cannot shed TNF α in response to an inflammatory challenge. Combined with our previous studies (Grieve et al. 2017), this work has changed our perspective on ADAM17, the central enzyme in cytokine and growth factor shedding. Our evidence implies that it would be more appropriate to consider it as the active subunit of a regulatory complex at the cell surface, where iRhoms provide regulatory functions (Maney et al., 2015, Cavadas et al., 2017, Grieve et al., 2017), and FRMD8 maintains the stability of the iRhom/ADAM17 complex post-ADAM17 maturation. It is essential that a pool of the sheddase is available on the cell surface to execute, for example, rapid cytokine release in response to inflammatory signals induced by bacterial infection.

In the only other paper about FRMD8 function, it was reported that FRMD8 (named Bili, after the *Drosophila* mutation) negatively regulates Wnt signalling by binding to the LRP6 co-receptor, thereby preventing the recruitment of the signal transduction protein axin (Kategaya et al., 2009). Although the signalling event being regulated is different, there is the obvious parallel that in both cases FRMD8 binds to the cytoplasmic tail of a transmembrane protein. In the case of Wnt signalling, this prevents the recruitment of axin; in the case of iRhom function, we do not yet know what the next step in the molecular chain of events is, but the cellular consequence is to prevent recruitment of iRhoms into the endolysosomal degradation system.

Our results extend an important theme to emerge from a number of studies, namely the significance of the iRhom cytoplasmic N-terminal region in regulating iRhom/ADAM17 function. Several reports indicate that N-terminal mutations in iRhoms cause complex phenotypes that combine aspects of gain and loss of iRhom function, which is consistent with a regulatory function for this region. First, the *cub* mutation, an N-terminal deletion in mouse iRhom2, does not abolish protein function but instead modulates it in complex ways that are still poorly understood (Hosur et al., 2014, Siggs et al., 2014). *cub* was described as a gain-

of-function mutation that leads to constitutively elevated release of amphiregulin, but is also reported to be defective in releasing TNF α (Hosur et al., 2014). Second, specific point mutations in the N-terminus of human iRhom2 are the cause of a rare genetic disorder called tylosis with oesophageal cancer (TOC) (Blaydon et al., 2012, Saarinen et al., 2012). TOC mutations, as well as truncation of parts of the N-terminus have been reported to enhance the activity of ADAM17 (Maney et al., 2015), leading to the conclusion that parts of the N-terminus have inhibitory functions on ADAM17 function. Third, phosphorylation of specific sites in the iRhom2 N-terminus result in 14-3-3 binding and consequent activation of substrate shedding by associated ADAM17 (Grieve et al., 2017, Cavadas et al., 2017), demonstrating that the N-terminus of iRhom2 also positively regulates ADAM17. The FRMD8 binding region does not overlap with these sites required for phosphorylation-dependent 14-3-3 binding, however it is formally possible that there is some functional overlap between them. We could not detect major changes in the interaction of FRMD8 with iRhom2 upon PMA stimulation (Figure 10-figure supplement 1), which leads to the phosphorylation of iRhoms (Grieve et al., 2017, Cavadas et al., 2017). Moreover, an iRhom2 mutant, in which 15 conserved phosphorylation sites have been mutated to alanine (iRhom2^{pDEAD}; Figure 3-figure supplement 1A) (Grieve et al., 2017), did not abolish the interaction with FRMD8 (Figure 10- figure supplement 1). This conclusively demonstrates that the binding of FRMD8 to iRhom2 does not require phosphorylation of iRhom2. However, it is still formally possible that phosphorylation of iRhom2 affects FRMD8 binding specifically at the cell surface. This change cannot be detected by analysing the entire iRhom2 pool, which is primarily localised in the early secretory pathway. Therefore, we cannot exclude that the phosphorylation state of the relatively small cell surface pool of iRhom2 regulates the interaction with FRMD8.

Consistent with our current results, we reported previously that iRhom2 lacking the entire N-terminus is not sufficient to support ADAM17-mediated shedding in iRhom1/2-deficient cells, although it can promote ER-to-Golgi trafficking of ADAM17 (Grieve et al., 2017). Complementary to the conclusion that iRhom N-termini are regulatory, the core TMD binding function of iRhoms depends on their membrane-embedded region (Grieve et al., 2017, Cavadas et al., 2017). A picture therefore begins to emerge of iRhoms having a modular structure, with a core, highly conserved TMD recognition domain in the membrane (and perhaps the lumen), regulated by a more variable N-terminal domain that can integrate cytoplasmic signals.

In light of the growing value of therapeutics that block TNF α signalling, and the wider potential of modulating a wide range of ADAM17 substrates, it is tempting to speculate that the cytoplasmic N-termini of iRhoms could provide potential new drug target opportunities. For example, the limited expression of iRhom2 makes it a theoretically attractive anti-

inflammatory target (Issuree et al., 2013, Lichtenthaler, 2013). iRhom2 knockout mice are broadly healthy, beyond defects in TNF α and type I interferon signalling that are only apparent upon challenge by bacterial and viral infections (McIlwain et al., 2012, Luo et al., 2016). Our work now implies that the interface between FRMD8 and iRhoms might be a useful target. This is supported, at least in principle, by our observation that even in cells with complete loss of FRMD8, there is still a low level of mature ADAM17 at the cell surface, and consequently residual TNF α shedding. Even very efficient pharmacological blocking of the FRMD8/iRhom interaction would not, therefore, fully abolish inflammatory responses, potentially reducing side effects. Consistent with this idea, mice with a hypomorphic mutation in ADAM17 (termed ADAM17^{ex/ex}) show that even only 5% of normal ADAM17 expression is sufficient to rescue many aspects of the loss of function phenotype (Chalaris et al., 2010). Moreover, a recent study has shown that reducing ADAM17 levels has great pharmaceutical potential: the reduced ADAM17 in the *Adam17*^{ex/ex} mouse is sufficient to limit colorectal cancer formation and any residual tumours are low-grade dysplasias (Schmidt et al., 2018).

In conclusion, our work demonstrates the cellular and physiological significance of FRMD8 binding to iRhoms, and how this stabilises the iRhom/ADAM17 sheddase complex at the cell surface. It also reinforces the picture that has begun to emerge of ADAM17 not acting alone but instead being supported by at least two other regulatory proteins that act as subunits of what is effectively an enzyme complex. This concept would help to explain how the activity of such a powerful and versatile – and therefore potentially dangerous – shedding enzyme is controlled with necessary precision. The next steps in fully revealing the role of FRMD8 will be to analyse the phenotypic consequences of its loss in mice, which should allow us to understand how the roles of FRMD8 roles in ADAM17 activation, Wnt signalling, and any other potential functions, are integrated. Notwithstanding these physiological questions, the work described here already provides a basis for beginning to investigate the potential of targeting the FRMD8/iRhom interface for modulating the release of ADAM17 substrates.

Materials and methods

Key Resources Table

Reagent type (species) or resource	Designation	Source or reference	Identifiers	Additional information
strain, strain	Frmd8 ^{-/-} : C57BL/6-	This paper	N/A	FRMD8 KO mice

background (mouse)	Frmd8 ^{tm1(KOMP)Vlcg}			generated as described in materials and methods
strain, strain background (mouse)	WT control: C57BL/6	This paper	N/A	WT control for FRMD8 KO mice
strain, strain background (mouse)	Rhbd12 ^{-/-} : C57BL/6- <i>Rhbd16</i> ^{A22}	(Adrain et al., 2012)	N/A	
cell line (human)	HEK293T cells	Freeman lab	RRID:CVCL_ 0063	
cell line (human)	HEK293T human iRhom1 ^{WT}	This paper	N/A	HEK293T cells transduced with pLEX.puro-human iRhom1WT-3xHA
cell line (human)	HEK293T human iRhom2 ^{WT}	This paper	N/A	HEK293T cells transduced with pLEX.puro-human iRhom2WT-3xHA
cell line (human)	HEK293T human UNC93B1	This paper	N/A	HEK293T cells transduced with pLEX.puro-human UNC93B1-3xHA
cell line (human)	HEK293T FRMD8 KO	This paper	N/A	CRISPR/Cas9- mediated KO cell line as described in materials and methods
cell line (human)	HEK293T FRMD8 KO + human iRhom2 ^{WT}	This paper	N/A	FRMD8 KO cells transduced with pLEX.puro-human iRhom2WT-3xHA
cell line (human)	HEK293T endogenous iRhom2-3xHA	This paper	N/A	CRISPR/Cas9- mediated knock-in cell line as described in

				materials and methods
cell line (human)	HEK293T iRhom1/iRhom2 double- knockout (DKO)	This paper	N/A	CRISPR/Cas9- mediated KO cell line as described in materials and methods
cell line (human)	HEK293T iRhom1/iRhom2 DKO + human iRhom2WT	This paper	N/A	DKO cells transduced with pLEX.puro-human iRhom2WT-3xHA
cell line (human)	HEK293T iRhom1/iRhom2 DKO + human iRhom2 Δ 300	This paper	N/A	DKO cells transduced with pLEX.puro-human iRhom2 Δ 300-3xHA
cell line (human)	HEK293T iRhom1/iRhom2 DKO + human FRMD8- iRhom2 Δ 300	This paper	N/A	DKO cells transduced with pLEX.puro-human FRMD8-iRhom2 Δ 300- 3xHA
cell line (human)	HEK293T iRhom1/iRhom2 DKO + human iRhom2 Δ 201- 300	This paper	N/A	DKO cells transduced with pLEX.puro-human iRhom2 Δ 201-300-3xHA
cell line (human)	hiPSC line AH017-13	(Fernandes et al., 2016)	James Martin Stem Cell Facility	
cell line (human)	hiPSC line AH017-13 FRMD8 KO clone 1 (clone F1)	This paper	N/A	CRISPR/Cas9- mediated KO cell line as described in materials and methods
cell line (human)	hiPSC line AH017-13 FRMD8 KO clone 2 (clone G6)	This paper	N/A	CRISPR/Cas9- mediated KO cell line as described in materials and methods
cell line (human)	hiPSC line AH017-13 WT (clone E4)	This paper	N/A	unedited WT control for FRMD8 KO iPSCs clones

cell line (mouse)	Frmd8 ^{-/-} ES cells: C57BL/6NTac- Frmd8 ^{tm1(KOMP)Vlcg} (clone 17364AC3)	KOMP	RRID:IMSR_K OMP:VG1736 4-1-Vlcg	
antibody	anti-β-actin-HRP, mouse monoclonal (clone AC- 15)	Sigma- Aldrich	Cat#A3854; RRID:AB_262 011	dilution is described in materials and methods
antibody	anti-ADAM10, mouse monoclonal (clone SHM14)	BioLegend	Cat#352702; RRID:AB_108 97813	dilution is described in materials and methods
antibody	anti-ADAM10, rabbit polyclonal	Cell Signaling Technology	Cat#14194	dilution is described in materials and methods
antibody	anti-ADAM17, mouse monoclonal (clone A300E)	(Yamamoto et al., 2012); received from Stefan Düsterhöft	N/A	dilution is described in materials and methods
antibody	anti-ADAM17, rabbit polyclonal	Abcam	Cat#ab39162; RRID:AB_722 565	dilution is described in materials and methods
antibody	anti-calnexin, rabbit polyclonal	Santa Cruz	Cat#sc- 11397; RRID:AB_224 3890	dilution is described in materials and methods
antibody	anti-FRMD8, rabbit polyclonal	Abcam	Cat#ab16993 3	dilution is described in materials and methods
antibody	anti-HA, rabbit polyclonal	Santa Cruz	Cat#sc-805; RRID:AB_631 618	dilution is described in materials and methods
antibody	anti-HA, rat monoclonal (clone 3F10)	Roche	Cat#1186742 3001; RRID:AB_100 94468	dilution is described in materials and methods

antibody	anti-HA tag, rabbit monoclonal (C29F4)	CST	Cat#3724; RRID:AB_1549585	dilution is described in materials and methods, used at 1:1000 for IF
antibody	anti-HA-HRP, rat monoclonal (clone 3F10)	Roche	Cat#12013819001; RRID:AB_390917	dilution is described in materials and methods
antibody	anti-iRhom2, rabbit polyclonal	(Adrain et al., 2012)	N/A	dilution is described in materials and methods
antibody	ant-LAMP1, mouse monoclonal (H4A3)	Santa Cruz	Cat#sc-20011; RRID:AB_626853	dilution is described in materials and methods, used at 1:250 for IF
antibody	anti-transferrin receptor 1, mouse monoclonal (clone H68.4)	Thermos Fisher Scientific	Cat#13-6800; RRID:AB_86623	dilution is described in materials and methods
antibody	anti-V5, goat polyclonal	Santa Cruz	Cat#sc-83849; RRID:AB_2019670	dilution is described in materials and methods, used at 1:1000 for IF
antibody	anti-goat-HRP, mouse monoclonal	Santa Cruz	Cat#sc-2354; RRID:AB_628490	dilution is described in materials and methods
antibody	anti-mouse-HRP, goat polyclonal	Santa Cruz	Cat#sc-2055; RRID:AB_631738	dilution is described in materials and methods
antibody	anti-rabbit-HRP, goat polyclonal	Sigma-Aldrich	Cat#A9169; RRID:AB_258434	dilution is described in materials and methods
antibody	anti-mouse Alexa Fluor 488, donkey polyclonal	Thermos Fisher Scientific	Cat#A-21202; RRID:AB_141607	dilution is described in materials and methods
antibody	anti-rabbit Alexa Fluor	Thermos	Cat#A-21206;	dilution is described in

	488, donkey polyclonal	Fisher Scientific	RRID:AB_2535792	materials and methods
antibody	anti-rabbit Alexa Fluor 647, donkey polyclonal	Thermos Fisher Scientific	Cat#A-31573; RRID:AB_2536183	dilution is described in materials and methods
recombinant DNA reagent	cDNA: human iRhom2 (NM_024599.2)	Origene	Cat#SC122961	
recombinant DNA reagent	cDNA: human FRMD8 (NM_031904)	Origene	Cat#SC107202	
recombinant DNA reagent	cDNA: human UNC93B1	(Brinkmann et al., 2007)	N/A	
recombinant DNA reagent	Plasmid: pLEX.puro	Thermo Fisher Scientific	Cat#OHS4735	
recombinant DNA reagent	Plasmid: pcDNA3.1(+)	Thermo Fisher Scientific	Cat#V790-20	
recombinant DNA reagent	Plasmid: entiviral packaging plasmid	(Adrain et al., 2012)	N/A	
recombinant DNA reagent	Plasmid: entiviral envelope plasmid	(Adrain et al., 2012)	N/A	
recombinant DNA reagent	Plasmid: pSpCas9(BB)-2A-Puro (pX459)	(Ran et al., 2013)	Addgene plasmid #48139	
recombinant DNA reagent	Plasmid: epX459(1.1)	received from Joey Rieosaame	N/A	
recombinant DNA reagent	Plasmid: pSpCas9(BB)-2A-Puro V2.0 (pX462 V2.0)	(Ran et al., 2013)	Addgene plasmid #62987	
transfected construct	Plasmid: pLEX.puro-human iRhom1WT-	(Christova et al., 2013)	N/A	

(human)	3xHA			
transfected construct (human)	Plasmid: pLEX.puro-human iRhom2WT-3xHA	This paper	N/A	cloned from human iRhom2 (NM_024599.2)
transfected construct (human)	Plasmid: pLEX.puro-human iRhom2Δ100-3xHA	This paper	N/A	human iRhom2 lacking amino acids 1-100
transfected construct (human)	Plasmid: pLEX.puro-human iRhom2Δ200-3xHA	This paper	N/A	human iRhom2 lacking amino acids 1-200
transfected construct (human)	Plasmid: pLEX.puro-human iRhom2Δ300-3xHA	This paper	N/A	human iRhom2 lacking amino acids 1-300
transfected construct (human)	Plasmid: pLEX.puro-human iRhom2Δ201-300-3xHA	This paper	N/A	human iRhom2 lacking amino acids 1-382
transfected construct (human)	Plasmid: pLEX.puro-human iRhom2Δ382-3xHA	This paper	N/A	human iRhom2 lacking amino acids 201-300
transfected construct (human)	Plasmid: pLEX.puro-human FRMD8-iRhom2Δ300-3xHA	This paper	N/A	human FRMD8 fused to human iRhom2Δ300 via a flexible linker (GSGSGS)
transfected construct (mouse)	Plasmid: pM6P.blast-mouse iRhom2 ^{WT} -3xHA	(Grieve et al., 2017)	N/A	
transfected construct (mouse)	Plasmid: pM6P.blast-mouse iRhom2 ^{cup} -3xHA	(Grieve et al., 2017)	N/A	
transfected construct (mouse)	Plasmid: pM6P.blast-mouse iRhom2 ^{pDEAD} -3xHA	(Grieve et al., 2017)	N/A	
sequence-	gRNA targeting exon 7	This paper	N/A	gRNA targeting exon 7

based reagent	of human FRMD8 (ACCCATAAAACGGCA GCTCGTGG)			of human FRMD8
sequence- based reagent	gRNA targeting exon 19 of human RHBDF2 (CCCAGCGGTCAGTG CAGCACCT)	This paper	N/A	gRNA targeting exon 19 of human RHBDF2
sequence- based reagent	gRNA targeting exon 3 of human RHBDF1 (GGAACCATGAGTGA GGCCCC)	This paper	N/A	gRNA targeting exon 3 of human RHBDF1
sequence- based reagent	gRNA targeting exon 3 of human RHBDF1 (GGGTGGCTTCTTGC GCTGCC)	This paper	N/A	gRNA targeting exon 3 of human RHBDF1
sequence- based reagent	gRNA targeting exon 10 of human RHBDF1 (AGCCGTGTGCATCTA TGGCC)	This paper	N/A	gRNA targeting exon 10 of human RHBDF1
sequence- based reagent	gRNA targeting exon 10 of human RHBDF1 (CCGTCTCATGCTGCG AGAAC)	This paper	N/A	gRNA targeting exon 10 of human RHBDF1
sequence- based reagent	gRNA targeting exon 2 of human RHBDF2 (GCAGAGCCGGAAGC CACCCC)	This paper	N/A	gRNA targeting exon 2 of human RHBDF2
sequence- based reagent	gRNA targeting exon 2 of human RHBDF2 (GGGTCTCTTTCTCGG GTGGC)	This paper	N/A	gRNA targeting exon 2 of human RHBDF2
sequence- based reagent	gRNA targeting exon 9 of human RHBDF2 (AAACTCGTCCATGTC ATCATCACC)	This paper	N/A	gRNA targeting exon 9 of human RHBDF2

sequence-based reagent	gRNA targeting exon of human RHBDF2 (ACGGGTGCGATGCC ATACGC)	This paper	N/A	gRNA targeting exon 9 of human RHBDF2
sequence-based reagent	non-targeting siGENOME control pool	Dharmacon	D-001206-13-50	
sequence-based reagent	siGENOME SMARTpool for human FRMD8	Dharmacon	M-018955-01-0010	
sequence-based reagent	siRNA targeting human RHBDF2 (HSS128594)	Thermo Fisher Scientific	Cat#1299001	
sequence-based reagent	siRNA targeting human RHBDF2 (HSS128595)	Thermo Fisher Scientific	Cat#1299001	
sequence-based reagent	Human <i>ACTB</i> (Hs99999903_m1)	Thermo Fisher Scientific	Cat#4331182	
sequence-based reagent	Human <i>ADAM17</i> (Hs01041915_m1)	Thermo Fisher Scientific	Cat#4331182	
sequence-based reagent	Human <i>FRMD8</i> (Hs00607699_mH)	Thermo Fisher Scientific	Cat#4331182	
sequence-based reagent	Human <i>RHBDF2</i> (Hs00226277_m1)	Thermo Fisher Scientific	Cat#4331182	
sequence-based reagent	Human <i>TNF</i> (Hs00174128_m1)	Thermo Fisher Scientific	Cat#4331182	
commercial assay or kit	BCA Protein Assay Kit	Thermo Fisher Scientific	Cat# 23225	

commercial assay or kit	Human TNF alpha ELISA Kit	Thermo Fisher Scientific	Cat#88-7346-86	
commercial assay or kit	SuperScript VILO cDNA synthesis kit	Thermo Fisher Scientific	Cat#11754050	
chemical compound, drug	1,10-Phenanthroline	Sigma-Aldrich	Cat#131377-5G	
chemical compound, drug	DSP (dithiobis(succinimidyl propionate))	Thermos Fisher Scientific	Cat#22585	
chemical compound, drug	EDTA-free protease inhibitor mix	Roche	Cat#11873580001	
chemical compound, drug	GW280264X (GW)	(Lorenzen et al., 2016); received from Stefan Düsterhöft	N/A	
chemical compound, drug	GI254023X (GI)	(Lorenzen et al., 2016); received from Stefan Düsterhöft	N/A	
chemical compound, drug	LPS	Sigma-Aldrich	Cat#L5668-2ML	
chemical compound, drug	nocodazole	Sigma-Aldrich	Cat#M1404	
chemical compound, drug	PNPP substrate	Thermos Fisher Scientific	Cat#34045	

chemical compound, drug	Rho kinase inhibitor Y-27632	Abcam	Cat#ab120129	
peptide, recombinant protein	Q5 High-Fidelity DNA polymerase	New England Biolabs	Cat#M0491S	
peptide, recombinant protein	Sequencing Grade Trypsin	Promega	Cat#V5111	
peptide, recombinant protein	HA peptide	Roche	Cat#l2149-.5MG	
peptide, recombinant protein	M-CSF	Gibco	Cat#PHC9501	
peptide, recombinant protein	IL-3	Gibco	Cat#PHC0033	
peptide, recombinant protein	BMP-4	Invitrogen	Cat#PHC9534	
peptide, recombinant protein	VEGF	PeproTech	Cat#100-20	
peptide, recombinant protein	SCF	Miltenyi	Cat#130-094-303	
peptide, recombinant protein	RhFGF (bFGF)	R&D	Cat#4114-TC	
other	anti-HA magnetic beads	Thermo Fisher Scientific	Cat#88837	

other	anti-V5 magnetic beads	MBL International	Cat#M167-11	
other	concanavalin A sepharose	Sigma- Aldrich	Cat#C9017- 25ML	
other	C18 spin columns	Thermo Fisher Scientific	Cat#89873	
other	vivaspin concentrator 500 (10,000 kDa MWCO)	Sartorius	Cat#VS0102	
other	mouse IgG agarose	Sigma- Aldrich	Cat#A0919- 5ML	
other	DMEM	Thermo Fischer Scientific	Cat#4196503 9	
other	Fetal bovine serum	Thermo Fischer Scientific	Cat#1050006 4	
other	Fish skin gelatin	Sigma- Aldrich	Cat#G7765	
other	KnockOut -DMEM	Thermo Fischer Scientific	Cat#10829	
other	KnockOut - serum replacement	Thermo Fischer Scientific	Cat#10828	
other	MEM Non-Essential Amino Acids (100x)	Thermo Fischer Scientific	Cat#11140- 035	
other	GlutaMAX (100x)	Thermo Fischer Scientific	Cat#35050- 038	

other	2-Mercaptoethanol (1000x)	Thermo Fischer Scientific	Cat#31350- 010	
other	Penicillin-Streptomycin (P/S 100x)	Thermo Fischer Scientific	Cat#15140- 122	
other	6-well ultra-low attachment plates	Corning	Cat#3471	
other	X-VIVO 15	Lonza	Cat#BE04- 418	
other	mTeSR1	Stemcell Technologies	Cat#12491	
other	Paraformaldehyde 16%	Electron Microscopy Sciences	Cat#15710	
other	hESC-qualified Geltrex	Thermo Fischer Scientific	Cat#A141330 2	
other	ProLong Gold antifade reagent with DAPI	Molecular Probes	Cat#P36935	
software, algorithm	FlowJo (version X 10.0.7r2)	FlowJo, LLC	https://www.fl owjo.com/solu tions/flowjo	
software, algorithm	Prism (version 7)	GraphPad	https://www.gr aphpad.com/s cientific- software/pris m/	
software, algorithm	MaxQuant (version 1.5.0.35)	(Cox and Mann, 2008)	http://www.co xdocs.org/dok u.php?id=max quant:start	

software, algorithm	Perseus (version 1.5.5.3)	(Tyanova et al., 2016)	http://www.coxdocs.org/doku.php?id=perseus:start	
software, algorithm	Fiji (version 2.0.0-rc-43/1.52a)	(Schindelin et al, 2012)	https://fiji.sc/	
software, algorithm	Clustal Omega	EMBL-EBI	https://www.ebi.ac.uk/Tools/msa/clustalo/	

476

477 *Molecular cloning*

478 Human UNC93B1, human iRhom2^{WT}, iRhom2^{Δ100}, iRhom2^{Δ200}, iRhom2^{Δ300}, iRhom2^{Δ382}
479 iRhom2^{Δ201-300}, and FRMD8-iRhom2^{Δ300} were amplified from human UNC93B1
480 (BC025669.1), human iRhom2 cDNA (NM_024599.2; Origene (SC122961)) and human
481 FRMD8 cDNA (NM_031904; Addgene (SC107202)) by PCR and cloned with an C-terminal
482 3xHA tag into the lentiviral vector pLEX.puro using Gibson assembly (New England Biolabs)
483 following the manufacturer's instructions. C-terminal V5-tagged FRMD8 (FRMD8-V5) was
484 amplified from human FRMD8 cDNA (Addgene (SC107202)) by PCR and cloned into
485 pcDNA3.1(+) using Gibson assembly. All constructs were verified by Sanger sequencing
486 (Source Bioscience, Oxford, UK).

487 pM6P.blast plasmids expressing mouse iRhom2^{WT}, iRhom2^{Δ268} (iRhom2 cub), and
488 iRhom2^{pDEAD} were described previously (Grieve et al., 2017).

489 *Transfection and transduction of cell lines*

490 Human embryonic kidney (HEK) 293T cells were cultured in DMEM (Sigma-Aldrich)
491 supplemented with 10% fetal calf serum (FCS) and 1x penicillin-streptomycin (PS) (all Gibco)
492 at 37°C with 5% CO₂. Cells were transiently transfected with DNA using FuGENE HD
493 (Promega). Per 10 cm² growth area 4 μl FuGENE HD was added to 1 μg DNA diluted in
494 OptiMEM (Gibco). The transfection mix was incubated for 20 min at room temperature and
495 added to cells. Protein expression was analysed 48 h - 72 h after transfection. For
496 knockdown experiments, siRNA was transfected using Lipofectamin RNAiMax (Invitrogen)
497 following the manufacturer's instructions. Per 6 well 50 pmol of FRMD8 SMARTpool siRNA
498 (Dharmacon; siGENOME Human FRMD8 (83786) siRNA; M-018955-01-0010), non-targeting
499 siRNA control pools (Dharmacon; siGENOME D-001206-13-50), RHBDF2 siRNA (Thermo

Fisher Scientific; HSS128594 and HSS128595) were used. Protein expression was analysed 72 h after transfection.

HEK293T wild-type cell lines stably expressing human UNC93B1-3xHA or human iRhom2-3xHA, and HEK293T iRhom1/2 DKO cell lines expressing iRhom2^{WT}, iRhom2^{Δ300}, iRhom2^{Δ201-300}, or FRMD8-iRhom2^{Δ300} were generated by lentiviral transduction using the pLEX.puro vector as described previously (Adrain et al., 2012). Cells were selected by adding 2.5 µg/ml puromycin (Gibco).

CRISPR/Cas9 genome editing in HEK293T cells

For CRISPR/Cas9-mediated knockout of FRMD8 the plasmid pSpCas9(BB)-2A-Puro (pX459; Addgene plasmid #48139) co-expressing the wild-type *Streptococcus pyogenes* Cas9 and the guide RNA (gRNA) was used. For gRNA design target sequences with a low chance of off targets were selected using online tools (<http://crispr.mit.edu>; <http://www.sanger.ac.uk/htgt/wge>). A gRNA targeting exon 7 (ACCCATAAAACGGCAGCTCG), which is present in all FRMD8 isoforms, was cloned into pX459. 1 µg plasmid was transfected into a 6-well of HEK293T cells. Cells were selected with puromycin 48 h after transfection to eliminate non-transfected cells. Single colonies were selected to establish clonal cell lines. Loss of FRMD8 expression was analysed by western blot and quantitative PCR.

HEK293T iRhom1/2 double-knockout cells were generated using the plasmid pSpCas9(BB)-2A-Puro V2.0 (pX462 V2.0) co-expressing the *S. pyogenes* Cas9 nickase mutant D10A and a guide gRNA. gRNAs targeting exon 3 (GGAACCATGAGTGAGGCCCC, GGGTGGCTTCTTGCCTGCC) and exon 10 (AGCCGTGTGCATCTATGGCC, CCGTCTCATGCTGCGAGAAC) of *RHBDF1*, and exon 2 (GCAGAGCCGGAAGCCACCCC, GGGTCTCTTTCTCGGGTGGC) and exon 9 (AACTCGTCCATGTCATCATCACC, ACGGGTGGCATGCCATACGC) of *RHBDF2* were individually cloned into pX462 V2.0. 250 ng of each plasmid were transfected together into a 6-well of HEK293T cells (8 plasmids in total per well). Cells were selected with puromycin 48 h after transfection and single colonies were selected to establish clonal cell lines. Loss of iRhom1 and iRhom2 was analysed by PCR.

To generate a knock-in of a triple HA tag at the C-terminus of endogenous iRhom2, a homology construct consisting of the triple HA tag (3xHA) flanked at both sides with homology arms of approximately 800 bp was cloned into pcDNA3.1(+). The *RHBDF2* locus was targeted in exon 19 in close proximity to the stop codon using a gRNA (AGCGGTCAGTGCAGCACCT or CAGCGGTCAGTGCAGCACC) cloned into vector

epX459(1.1) (generated by subcloning enhanced Cas9 (eSpCas9) v1.1 into plasmid pX459; a kind gift from Dr Joey Riepsaame, University of Oxford). HEK293T cells were treated with 200 ng/ml nocodazole (Sigma-Aldrich) for 17 h and then transfected with epX459(1.1) and the pcDNA3.1(+) homology plasmid (0.5 µg each per 6-well). After puromycin selection and single cell cloning, cell clones were tested for the insertion of the 3xHA tag by PCR.

HEK293 ADAM17 knockout cells were kindly provided by Dr Stefan Düsterhöft and have been published previously (Riethmueller et al., 2016).

Mass spectrometry and data analysis

HEK293T cells expressing human UNC93B1-3xHA (control) and human iRhom2-3xHA were used for anti-HA co-immunoprecipitation and analysed by mass spectrometry as described previously (Grieve et al., 2017). Peptides were injected into a nano-flow reversed-phase liquid chromatography coupled to Q Exactive Hybrid Quadrupole-Orbitrap mass spectrometer (Thermo Scientific). The raw data files generated were processed using the MaxQuant (version 1.5.0.35) software, integrated with the Andromeda search engine as described previously (Cox and Mann, 2008, Cox et al., 2011). Differential protein abundance analysis was performed with Perseus (version 1.5.5.3). A two-sample t-test was used to assess the statistical significance of protein abundance fold-changes. P-values were adjusted for multiple hypothesis testing with the Benjamini-Hochberg correction (Hochberg and Benjamini, 1990).

Co-immunoprecipitation

Cells were washed with ice-cold PBS and then lysed on ice in Triton X-100 lysis buffer (1% Triton X-100, 150 mM NaCl, 50 mM Tris-HCl pH 7.5) supplemented with EDTA-free protease inhibitor mix (Roche) and 10 mM 1,10-Phenanthroline (Sigma-Aldrich). Cell debris were pelleted by centrifugation at 20,000 g at 4°C for 10 min. Proteins were immunoprecipitated by incubation with anti-HA magnetic beads (Thermo Scientific) or anti-V5 magnetic beads (MBL International) for 1 h at 4°C. Beads were washed with Triton X-100 wash buffer (1% Triton X-100, 300 mM NaCl, 50 mM Tris-HCl pH 7.5). Proteins were eluted in 2x LDS buffer (life technologies) supplemented with 50 mM DTT for 10 min at 65°C.

Concanavalin A enrichment

N-glycosylated proteins were enriched by incubating cells lysates with concanavalin A sepharose (Sigma-Aldrich) at 4°C for at least 3 h with over-head rotation. Beads were pelleted (2,500 g, 5 min, 4°C) and washed with Triton X-100 wash buffer. Proteins were eluted in 2x LDS buffer supplemented with 50 mM DTT and 50% sucrose for 10 min at 65°C.

567 *Cycloheximide chase*

568 To access protein stability, HEK293T cells were treated with 100 µg/ml cycloheximide
569 (CHX; Sigma-Aldrich) for 0 h – 8 h to block protein synthesis. After incubation, cells were
570 washed with ice-cold PBS and then lysed on ice in Triton X-100 lysis buffer supplemented
571 with EDTA-free protease inhibitor mix and 10 mM 1,10-Phenanthroline. Lysates were
572 centrifuged at 20,000 g at 4°C for 10 min and analysed by SDS-PAGE.

573 *SDS-PAGE and western blotting*

574 Cell lysates were mixed with 4x LDS buffer (life technologies) supplemented with
575 50 mM DTT and denatured for 10 min at 65°C prior to loading on 4-12% Bis-Tris gradient
576 gels run in MOPS running buffer (both Invitrogen). Proteins were transferred to a
577 polyvinylidene difluoride (PVDF) membrane (Millipore) in transfer buffer (Invitrogen). The
578 membrane was blocked in 5% milk-TBST (150 mM NaCl, 10 mM Tris-HCl pH 7.5, 0.05%
579 Tween 20, 5% dry milk powder) and then incubated with the primary antibody: mouse
580 monoclonal anti-β-actin-HRP (Sigma-Aldrich, A3854, 1:5000), rabbit polyclonal anti-ADAM17
581 (abcam; ab39162; 1:2000), rabbit polyclonal anti-FRMD8 (abcam; ab169933; 1:500), rat
582 monoclonal anti-HA-HRP (Roche, 11867423001, 1:2000), goat polyclonal anti-V5 (Santa
583 Cruz, sc-83849, 1:2000), mouse monoclonal anti-transferrin receptor 1, (Thermo Fisher
584 Scientific, 13-6800, 1:2000), and rabbit polyclonal anti-iRhom2 ((Adrain et al., 2012); 1:500).
585 After three washing steps with TBST (150 mM NaCl, 10 mM Tris-HCl pH 7.5, 0.05% Tween
586 20), membranes were incubated with the secondary antibody for 1 h at room temperature
587 using either goat polyclonal anti rabbit-HRP (Sigma-Aldrich, A9169, 1:20000), mouse
588 monoclonal anti-goat-HRP (Santa Cruz, sc-2354, 1:5000) or goat polyclonal anti-mouse-HRP
589 (Santa Cruz, sc-2055, 1:5000).

590 *mRNA isolation and quantitative RT-PCR*

591 Cells were harvested in PBS and pelleted at 3000 g, 5 min, 4°C. RNA was isolated
592 using the RNeasy kit (Qiagen) and reverse transcribed using the SuperScript VILO cDNA
593 synthesis kit (Invitrogen). Resulting cDNA was used for quantitative PCR (qPCR) using the
594 TaqMan Gene Expression Master Mix (Applied Biosystems) and the following TaqMan
595 probes (all Thermo Fisher Scientific): human ACTB (Hs99999903_m1), human FRMD8
596 (Hs00607699_mH), human RHBDF2 (Hs00226277_m1), and human TNFα
597 (Hs00174128_m1). qPCR was performed on a StepOnePlus system (Applied Biosystems).
598 Gene expression was normalized to ACTB expression and expressed as relative quantities
599 compared to the corresponding wild-type cell line. Error bars indicate the standard derivation
600 of technical replicates.

601 *Shedding assay*

602 8 x 10⁴ HEK293T cells were seeded in triplicates per condition into poly-(L)-lysine (PLL;
603 Sigma-Aldrich)-coated 24-well plates and transfected the next day with 30 ng plasmid DNA
604 encoding Alkaline Phosphatase (AP)-conjugated AREG, HB-EGF or TGF α (received from
605 Prof Carl Blobel). 48 h after transfection, cells were washed with OptiMEM and then
606 incubated with 200 μ l phenolred-free OptiMEM (Gibco) containing either 200 nM PMA, the
607 corresponding volume of the solvent (DMSO), or 200 nM PMA and 1 μ M GW (synthesized
608 by Iris Biotech (Marktredwitz, Germany) and kindly provided by Dr Stefan Düsterhöft) for 30
609 min at 37°C. Cell supernatants were collected, the cells were washed in PBS and lysed in
610 200 μ l Triton X-100 lysis buffer. The activity of AP in cell lysates and supernatants was
611 determined by incubating 100 μ l AP substrate p-nitrophenyl phosphate (PNPP) (Thermo
612 Scientific) with 100 μ l cell lysate or cell supernatant at room temperature followed by the
613 measurement of the absorption at 405 nm. The percentage of AP-conjugated material
614 released from each well was calculated by dividing the signal from the supernatant by the
615 sum of the signal from lysate and supernatant. The data was expressed as mean of at least
616 three independent experiments, each of which contained three biological replicates per
617 condition.

618 *Deglycosylation assay*

619 Cells were lysed in Triton X-100 lysis buffer as described above. Lysates were first
620 denatured with Glycoprotein Denaturing Buffer (New England Biolabs) at 65°C for 15 min
621 and then treated with endoglycosidase H (Endo H) or peptide:N-glycosidase F (PNGase F)
622 following the manufacturer's instructions (New England Biolabs).

623 *Flow cytometry*

624 For ADAM10 and ADAM17 cell surface staining, HEK293T cells were stimulated with
625 200 nM PMA for 5 min before harvest in PBS. 0.5 x 10⁶ HEK293T cells were washed with
626 ice-cold FACS buffer (0.25% BSA, 0.1 % sodium azide in PBS) and stained with rabbit
627 polyclonal anti-HA antibody (Santa Cruz, sc-805; 0.5 μ g diluted in FACS buffer), mouse
628 monoclonal anti-ADAM10 (Biolegend, 352702; 4 μ g diluted in FACS buffer) or mouse
629 monoclonal anti-ADAM17 (A300E antibody (Yamamoto et al., 2012), kindly provided by Dr
630 Stefan Düsterhöft; 8 μ g diluted in FACS buffer) on ice for 45 min. After two washes with
631 FACS buffer, the cells were incubated with Alexa Fluor 488-coupled secondary antibody
632 (Invitrogen, A21202 or A21206); 1:1000 dilution in FACS buffer) on ice for 30 min. Cells were
633 washed twice with ice-cold FACS buffer and then analysed with a BD FACSCalibur (BD

Biosciences) and FlowJo software. Cells stained only with the secondary antibody or anti-HA negative cells served as control.

Immunofluorescence staining and confocal microscopy

HEK293T iRhom1/2 DKO cells (1.5×10^5) transduced with indicated iRhom2 constructs were plated on 13 mm PLL-coated glass coverslips in 12-well dishes. In FRMD8-V5 or TACE-V5 overexpression experiments, cells were transfected with 200 ng vector and grown for 72 h prior to fixation. As indicated, cells were treated with 100 nM bafilomycin for 16 h before fixation, to inhibit lysosomal degradation. Cells were washed three times in PBS at room temperature and fixed with 4% paraformaldehyde in PBS at room temperature for 20 mins. Fixative was quenched with 50 mM NH_4Cl for 5 min. Cells were permeabilised in 0.2% Triton X-100 in PBS for 30 min and epitopes blocked with 1% fish-skin gelatin (Sigma-Aldrich) in PBS for 1 h. Coverslips were then incubated at room temperature for 2 h with rabbit anti-HA tag (Cell Signalling, 3724) and goat anti-V5 probe (Santa Cruz, sc-83849) in 1% fish-skin gelatin/PBS. After three PBS washes, coverslips were incubated with Alexa Fluor-coupled secondary antibodies raised in donkey (Invitrogen) for 45 min at room temperature. Cells were subsequently washed three times with PBS and once with H_2O , prior to mounting on glass slides with mounting medium containing DAPI (ProLong Gold; ThermoFisher Scientific). Images were acquired with a laser scanning confocal microscope (Fluoview FV1000; Olympus) with a 60x1.4 NA oil objective and processed using Fiji (ImageJ).

Culture of human iPSCs

To generate iPSC-derived FRMD8 knockout macrophages, the human iPSC line AH017-13 was used. The AH017-13 line was derived from dermal fibroblasts of healthy donor in the James Martin Stem Cell Facility, University of Oxford as published previously (Fernandes et al., 2016). Donors had given signed informed consent for the derivation of human iPSC lines from skin biopsies and SNP analysis (Ethics Committee: National Health Service, Health Research Authority, NRES Committee South Central, Berkshire, UK (REC 10/H0505/71)). AH017-13 iPSCs were cultured feeder cell-free in mTeSR1 (STEMCELL Technologies) on hESC-qualified geltrex (Gibco). iPSCs were fed daily and routinely passaged with 0.5 mM EDTA, or when required using TrypLE (Gibco) and plated in media containing 10 $\mu\text{mol/l}$ Rho-kinase inhibitor Y-27632 (Abcam).

Genome editing of iPSCs lines

AH017-13 iPSCs were transfected by electroporation using the Neon Transfection System (Invitrogen). 3×10^6 AH017-13 iPSCs were electroporated (1400 mV, 20 ms, 1

pulse) in a 100 µl tip with 15 µg pX459-FRMD8-exon7 plasmid DNA (endotoxin-free quality), then plated at a density of 4×10^5 cells/cm² and selected 48 h after transfection with 0.25 µg/ml puromycin. After 48 h of selection, surviving cells were plated on a feeder-layer of 4×10^6 irradiated mouse embryonic fibroblasts (MEFs) in 0.1% gelatin-coated 10 cm culture dishes and cultured in hES medium (KnockOut DMEM, 20% KnockOut serum replacement, 2 mM L-Glutamine, 100 µM nonessential amino acids, 50 µM 2-Mercaptoethanol (all Gibco) and 10 ng/mL basic fibroblastic growth factor (bFGF, R&D)). Colonies were manually selected and grown on geltrex in mTeSR1. Clones were analysed by western blot using the anti-FRMD8 antibody, and PCR followed by Sanger sequencing. For PCR DNA was isolated from iPSCs by incubation in DNA isolation buffer (10 mM Tris-HCl (pH 8), 1 mM EDTA, 25 mM NaCl, 200 µg/ml proteinase K added freshly) at 65°C for 30 min. Proteinase K was inactivated at 95°C for 2 min. PCR using Q5 polymerase was performed according to the manufacturer's instructions (New England Biolabs) using primers FRMD8_fw (TGCAGATCCATGACGAGGA) and FRMD8_rev (GTGCTCGTGACAAGACAC). The PCR product was purified and sequenced using the primer FRMD8_exon7_fw (GCCAGAGTCTCTTTGCTG) for Sanger sequencing (Source Bioscience, Oxford).

Differentiation of iPSCs into macrophages

AH017-13 wild-type and FRMD8 knockout clones were analysed by Illumina HumanOmniExpress24 single nucleotide polymorphism (SNP) array at the Wellcome Trust Centre for Human Genetics at the University of Oxford and assessed using KaryoStudio software to confirm normal karyotypes before differentiation into macrophages. For this study iPSCs were differentiated into embryoid bodies (EBs) by mechanical lifting of iPSC colonies and differentiated into macrophages as described in (van Wilgenburg et al., 2013). Briefly, iPSCs were grown on a feeder layer of MEFs in hES medium. A dense 10 cm² well of iPSCs was scored into 10x 10 sections using a plastic pipette tip. The resulting 100 patches were lifted with a cell scraper and cell clumps were transferred into a 6-well ultra-low adherence plate (Corning) containing EB formation medium (hES medium supplemented with 50ng/ml BMP4 (Invitrogen), 50ng/ml VEGF (Peprotech) and 20 ng/ml SCF (Miltentyi)) to form EBs. A 50% medium change was performed every second day. On day 5 EBs were harvested. Approximately 60-80 EBs were transferred into a T75 flask containing factory medium (X-VIVO 15 (Lonza) supplemented with 2 mM L-Glutamine, 50 µM 2-Mercaptoethanol, 100 ng/ml M-CSF and 25 ng/mL IL-3, 100 U/ml penicillin and 100 µg/ml streptomycin (all Gibco)). The EBs were fed weekly with fresh factory medium. After approximately two weeks EBs started to produce non-adherent macrophage precursors, which were harvested from the supernatant of EB cultures through a 70 µm cell strainer. Cells were differentiated into

703 mature adherent macrophages for 7 days in macrophage medium (X-VIVO 15 supplemented
704 with 2 mM L-Glutamine, 100 ng/ml M-CSF, 100 U/ml penicillin and 100 µg/ml streptomycin).

705 *ELISA*

706 iPSC-derived macrophages were harvested from EB cultures, counted and seeded at
707 25,000 cells per well into 96-well tissue culture plates in triplicates per condition.
708 Macrophages were cultured in macrophage differentiation medium for 7 days, and then
709 activated with 50 ng/ml LPS (Sigma-Aldrich) in fresh macrophage differentiation medium for
710 4 h. For inhibitor treatments cells were incubated with 50 ng/ml LPS and 3 µM GW or GI
711 (synthesized by Iris Biotech (Marktredwitz, Germany) and kindly provided by Dr Stefan
712 Düsterhöft) for 4 h. Cell culture supernatants were collected and cleared from cells by
713 centrifugation. TNFα in supernatants was measured by ELISA (Human TNF alpha ELISA
714 Ready-SET-Go, eBioscience (88-7346-86)) according to the manufacturer's instructions.
715 Macrophages were lysed in Triton X-100 lysis buffer and protein concentration was
716 determined using a BCA assay (Thermo Scientific). The amount of TNFα in the supernatant
717 was normalised to the protein concentration of the corresponding cell lysate to adjust for
718 differences in TNFα release due to cell numbers.

719 *Mouse work*

720 Commercially available *Frmd8*^{-/-} mouse ES cells from KOMP Repository at UC Davis
721 were used to generate *Frmd8*^{-/-} mice. The mouse ES cells (C57BL/6NTac strain) were
722 injected into blastocysts of Balb/c mice. Chimeras were bred to C57BL/6 to generate
723 *Frmd8*^{+/-} mice that were used for breeding of the colony and the generation of *Frmd8*^{-/-} mice.
724 For mice described in Figure 9-figure supplement 2B, we excised the LoxP-flanked neomycin
725 resistance gene by breeding *Frmd8*^{-/-} mice with homozygous Sox2-Cre deleter strain mice.
726 The mouse work was performed under project licenses 80/2584 and 30/2306. Mouse tissues
727 were collected from sacrificed animals and stored on dry ice or at -80°C. Tissues were lysed
728 in Triton X-100 RIPA buffer (1% Triton X-100, 150 mM NaCl, 50 mM Tris-HCl (pH 7.5), 0.1%
729 SDS, 0.5% sodium deoxycholate) supplemented with EDTA-free protease inhibitor mix and
730 10 mM 1,10-Phenanthroline using a tissue homogeniser (Omni International). Lysates were
731 cleared from cell debris by centrifugation (20,000 g, 4°C, 10 min). Protein concentrations of
732 tissue lysates were determined using a BCA assay.

733 *Statistical analysis and data presentation*

734 Values are expressed as means of at least three independent experiments with error
735 bars representing the standard deviation. Unpaired, two-tailed t-tests were used for statistical

analysis. Shedding assays and ELISA data was analysed using a Mann-Whitney test. Flow cytometry blots shown represent one from at least three experiments with similar outcome.

Ethics statement

Human iPSC lines were derived from dermal fibroblasts of donors that had given signed informed consent for the derivation of human iPSC lines from skin biopsies and SNP analysis (Ethics Committee: National Health Service, Health Research Authority, NRES Committee South Central, Berkshire, UK (REC 10/H0505/71)).

All procedures on mice were conducted in accordance with the UK Scientific Procedures Act (1986) under a project license (PPL) authorized by the UK Home Office Animal Procedures Committee, project licenses 80/2584 and 30/2306, and approved by the Sir William Dunn School of Pathology Local Ethical Review Committee.

Cell lines statement

We used HEK293T cells (RRID: CVCL_0063) for analysis of protein-protein interactions, subcellular localisation and loss-of-function experiments. These cells were used for experiments that provided a strong platform of *in vitro* evidence of a relationship between FRMD8 and iRhoms, prior to the generation of iPSC-derived macrophages and FRMD8 knock-out mice. All HEK293T-based cell lines have been tested negative for mycoplasma contamination and were previously reported in Grieve AG et al., 2017. eLife.

Acknowledgements

We gratefully acknowledge the support of Oxford's Advanced Proteomics Facility for our mass spectrometry based proteomic screen and Monika Stegmann for statistical analysis of the results. We also thank Genome Engineering Oxford, specifically Joey Riepsaame and Andrew Bassett, who helped us to design and clone guide RNAs for CRISPR/enhanced Cas9 gene editing. We are thankful for the assistance in animal work from the staff of the mouse facility and for support from Elizabeth Robertson, Jonathan Godwin, Angela Moncada Pazos, and Clémence Levet. Immunofluorescent microscopy was performed in Oxford's Micron imaging facility. We thank members of the Freeman lab for their extensive support throughout this project and their advice on the manuscript. We also thank Stefan Düsterhöft for providing reagents. This research was supported by the Wellcome Trust to MF (grant number 101035/Z/13/Z). The James Martin Stem Cell Facility has received support from the Wellcome Trust ISSF (121302) and MRC (MC_EX_MR/N50192X/1). UK is supported by the Medical Research Council (award number 1374214) and a Boehringer Ingelheim Fonds PhD fellowship. AG received funding from the European Union's Horizon 2020 research and innovation programme under the Marie Skłodowska-Curie grant agreement No 659166. BS is supported by the Medical Research Council and a Boehringer Ingelheim Fonds PhD fellowship.

Conflict of interest

The authors have no conflict of interest.

References

- ADRAIN, C., ZETTL, M., CHRISTOVA, Y., TAYLOR, N. & FREEMAN, M. 2012. Tumor necrosis factor signaling requires iRhom2 to promote trafficking and activation of TACE. *Science*, 335, 225-8.
- BLACK, R. A., RAUCH, C. T., KOZLOSKY, C. J., PESCHON, J. J., SLACK, J. L., WOLFSON, M. F., CASTNER, B. J., STOCKING, K. L., REDDY, P., SRINIVASAN, S., NELSON, N., BOIANI, N., SCHOOLEY, K. A., GERHART, M., DAVIS, R., FITZNER, J. N., JOHNSON, R. S., PAXTON, R. J., MARCH, C. J. & CERRETTI, D. P. 1997. A metalloproteinase disintegrin that releases tumour-necrosis factor-alpha from cells. *Nature*, 385, 729-33.
- BLAYDON, D. C., ETHERIDGE, S. L., RISK, J. M., HENNIES, H. C., GAY, L. J., CARROLL, R., PLAGNOL, V., MCRONALD, F. E., STEVENS, H. P., SPURR, N. K., BISHOP, D. T., ELLIS, A., JANKOWSKI, J., FIELD, J. K., LEIGH, I. M., SOUTH, A. P. & KELSELL, D. P. 2012. RHBDF2 mutations are associated with tylosis, a familial esophageal cancer syndrome. *Am J Hum Genet*, 90, 340-6.
- CAVADAS, M., OIKONOMIDI, I., GASPAR, C. J., BURBRIDGE, E., BADENES, M., FELIX, I., BOLADO, A., HU, T., BILECK, A., GERNER, C., DOMINGOS, P. M., VON KRIEGSHEIM, A. & ADRAIN, C. 2017. Phosphorylation of iRhom2 Controls Stimulated Proteolytic Shedding by the Metalloprotease ADAM17/TACE. *Cell Rep*, 21, 745-757.

- CHALARIS, A., ADAM, N., SINA, C., ROSENSTIEL, P., LEHMANN-KOCH, J., SCHIRMACHER, P., HARTMANN, D., CICHY, J., GAVRILOVA, O., SCHREIBER, S., JOSTOCK, T., MATTHEWS, V., HASLER, R., BECKER, C., NEURATH, M. F., REISS, K., SAFTIG, P., SCHELLER, J. & ROSE-JOHN, S. 2010. Critical role of the disintegrin metalloprotease ADAM17 for intestinal inflammation and regeneration in mice. *J Exp Med*, 207, 1617-24.
- CHRISTOVA, Y., ADRAIN, C., BAMBROUGH, P., IBRAHIM, A. & FREEMAN, M. 2013. Mammalian iRhoms have distinct physiological functions including an essential role in TACE regulation. *EMBO Rep*, 14, 884-90.
- COX, J. & MANN, M. 2008. MaxQuant enables high peptide identification rates, individualized p.p.b.-range mass accuracies and proteome-wide protein quantification. *Nature Biotechnology*, 26, 1367-1372.
- COX, J., NEUHAUSER, N., MICHALSKI, A., SCHELTEMA, R. A., OLSEN, J. V. & MANN, M. 2011. Andromeda: A Peptide Search Engine Integrated into the MaxQuant Environment. *Journal of Proteome Research*, 10, 1794-1805.
- ENDRES, K., ANDERS, A., KOJRO, E., GILBERT, S., FAHRENHOLZ, F. & POSTINA, R. 2003. Tumor necrosis factor-alpha converting enzyme is processed by proprotein-convertases to its mature form which is degraded upon phorbol ester stimulation. *European Journal of Biochemistry*, 270, 2386-2393.
- FERNANDES, H. J., HARTFIELD, E. M., CHRISTIAN, H. C., EMMANOULIDOU, E., ZHENG, Y., BOOTH, H., BOGETOFTE, H., LANG, C., RYAN, B. J., SARDI, S. P., BADGER, J., VOWLES, J., EVETTS, S., TOFARIS, G. K., VEKRELLIS, K., TALBOT, K., HU, M. T., JAMES, W., COWLEY, S. A. & WADE-MARTINS, R. 2016. ER Stress and Autophagic Perturbations Lead to Elevated Extracellular alpha-Synuclein in GBA-N370S Parkinson's iPSC-Derived Dopamine Neurons. *Stem Cell Reports*, 6, 342-56.
- FREEMAN, M. 2014. The rhomboid-like superfamily: molecular mechanisms and biological roles. *Annu Rev Cell Dev Biol*, 30, 235-54.
- GRIEVE, A. G., XU, H., KUNZEL, U., BAMBROUGH, P., SIEBER, B. & FREEMAN, M. 2017. Phosphorylation of iRhom2 at the plasma membrane controls mammalian TACE-dependent inflammatory and growth factor signalling. *Elife*, 6.
- HOCHBERG, Y. & BENJAMINI, Y. 1990. More Powerful Procedures for Multiple Significance Testing. *Statistics in Medicine*, 9, 811-818.
- HOSUR, V., JOHNSON, K. R., BURZENSKI, L. M., STEARNS, T. M., MASER, R. S. & SHULTZ, L. D. 2014. Rhbdf2 mutations increase its protein stability and drive EGFR hyperactivation through enhanced secretion of amphiregulin. *Proc Natl Acad Sci U S A*, 111, E2200-9.
- ISSUREE, P. D., MARETZKY, T., MCILWAIN, D. R., MONETTE, S., QING, X., LANG, P. A., SWENDEMAN, S. L., PARK-MIN, K. H., BINDER, N., KALLIOLIAS, G. D., YARILINA, A., HORIUCHI, K., IVASHKIV, L. B., MAK, T. W., SALMON, J. E. & BLOBEL, C. P. 2013. iRHOM2 is a critical pathogenic mediator of inflammatory arthritis. *J Clin Invest*, 123, 928-32.
- JOHNSON, K. R., LANE, P. W., COOK, S. A., HARRIS, B. S., WARD-BAILEY, P. F., BRONSON, R. T., LYONS, B. L., SHULTZ, L. D. & DAVISSON, M. T. 2003. Curly bare (cub), a new mouse mutation on chromosome 11 causing skin and hair abnormalities, and a modifier gene (mcub) on chromosome 5. *Genomics*, 81, 6-14.
- KALLIOLIAS, G. D. & IVASHKIV, L. B. 2016. TNF biology, pathogenic mechanisms and emerging therapeutic strategies. *Nat Rev Rheumatol*, 12, 49-62.
- KATEGAYA, L. S., CHANGKAKOTY, B., BIECHELE, T., CONRAD, W. H., KAYKAS, A., DASGUPTA, R. & MOON, R. T. 2009. Bili inhibits Wnt/beta-catenin signaling by regulating the recruitment of axin to LRP6. *PLoS One*, 4, e6129.
- KOEHN, J., HUESKEN, D., JARITZ, M., ROT, A., ZURINI, M., DWERTMANN, A., BEUTLER, B. & KORTHAUER, U. 2007. Assessing the function of human UNC-93B in Toll-like receptor signaling and major histocompatibility complex II response. *Hum Immunol*, 68, 871-8.
- LI, X., MARETZKY, T., WESKAMP, G., MONETTE, S., QING, X., ISSUREE, P. D., CRAWFORD, H. C., MCILWAIN, D. R., MAK, T. W., SALMON, J. E. & BLOBEL, C.

P. 2015. iRhoms 1 and 2 are essential upstream regulators of ADAM17-dependent EGFR signaling. *Proc Natl Acad Sci U S A*, 112, 6080-5.

LICHTENTHALER, S. F. 2013. iRHOM2 takes control of rheumatoid arthritis. *J Clin Invest*, 123, 560-2.

LUO, W. W., LI, S., LI, C., LIAN, H., YANG, Q., ZHONG, B. & SHU, H. B. 2016. iRhom2 is essential for innate immunity to DNA viruses by mediating trafficking and stability of the adaptor STING. *Nat Immunol*, 17, 1057-66.

MANEY, S. K., MCILWAIN, D. R., POLZ, R., PANDYRA, A. A., SUNDARAM, B., WOLFF, D., OHISHI, K., MARETZKY, T., BROOKE, M. A., EVERS, A., VASUDEVAN, A. A., AGHAEPOUR, N., SCHELLER, J., MUNK, C., HAUSSINGER, D., MAK, T. W., NOLAN, G. P., KELSELL, D. P., BLOBEL, C. P., LANG, K. S. & LANG, P. A. 2015. Deletions in the cytoplasmic domain of iRhom1 and iRhom2 promote shedding of the TNF receptor by the protease ADAM17. *Sci Signal*, 8, ra109.

MCILWAIN, D. R., LANG, P. A., MARETZKY, T., HAMADA, K., OHISHI, K., MANEY, S. K., BERGER, T., MURTHY, A., DUNCAN, G., XU, H. C., LANG, K. S., HAUSSINGER, D., WAKEHAM, A., ITIE-YOUTEN, A., KHOKHA, R., OHASHI, P. S., BLOBEL, C. P. & MAK, T. W. 2012. iRhom2 regulation of TACE controls TNF-mediated protection against *Listeria* and responses to LPS. *Science*, 335, 229-32.

MONACO, C., NANCHAHAL, J., TAYLOR, P. & FELDMANN, M. 2015. Anti-TNF therapy: past, present and future. *Int Immunol*, 27, 55-62.

MOSS, M. L., JIN, S. L., MILLA, M. E., BICKETT, D. M., BURKHART, W., CARTER, H. L., CHEN, W. J., CLAY, W. C., DIDSBURY, J. R., HASSLER, D., HOFFMAN, C. R., KOST, T. A., LAMBERT, M. H., LEESNITZER, M. A., MCCAULEY, P., MCGEEHAN, G., MITCHELL, J., MOYER, M., PAHEL, G., ROCQUE, W., OVERTON, L. K., SCHOENEN, F., SEATON, T., SU, J. L., BECHERER, J. D. & ET AL. 1997. Cloning of a disintegrin metalloproteinase that processes precursor tumour-necrosis factor- α . *Nature*, 385, 733-6.

NAKAGAWA, T., GUICHARD, A., CASTRO, C. P., XIAO, Y., RIZEN, M., ZHANG, H. Z., HU, D., BANG, A., HELMS, J., BIER, E. & DERYNCK, R. 2005. Characterization of a human rhomboid homolog, p100hRho/RHBDF1, which interacts with TGF- α family ligands. *Dev Dyn*, 233, 1315-31.

RIETHMUELLER, S., EHLERS, J. C., LOKAU, J., DUSTERHOFT, S., KNITTLER, K., DOMBROWSKY, G., GROTZINGER, J., RABE, B., ROSE-JOHN, S. & GARBERS, C. 2016. Cleavage Site Localization Differentially Controls Interleukin-6 Receptor Proteolysis by ADAM10 and ADAM17. *Sci Rep*, 6, 25550.

ROSE-JOHN, S. 2013. ADAM17, shedding, TACE as therapeutic targets. *Pharmacological Research*, 71, 19-22.

SAARINEN, S., VAHTERISTO, P., LEHTONEN, R., AITTO MAKI, K., LAUNONEN, V., KIVILUOTO, T. & AALTONEN, L. A. 2012. Analysis of a Finnish family confirms RHBDF2 mutations as the underlying factor in tylosis with esophageal cancer. *Fam Cancer*, 11, 525-8.

SAHIN, U. & BLOBEL, C. P. 2007. Ectodomain shedding of the EGF-receptor ligand epigen is mediated by ADAM17. *FEBS Lett*, 581, 41-4.

SAHIN, U., WESKAMP, G., KELLY, K., ZHOU, H. M., HIGASHIYAMA, S., PESCHON, J., HARTMANN, D., SAFTIG, P. & BLOBEL, C. P. 2004. Distinct roles for ADAM10 and ADAM17 in ectodomain shedding of six EGFR ligands. *J Cell Biol*, 164, 769-79.

SCHLONDORFF, J., BECHERER, J. D. & BLOBEL, C. P. 2000. Intracellular maturation and localization of the tumour necrosis factor α convertase (TACE). *Biochem J*, 347 Pt 1, 131-8.

SCHMIDT, S., SCHUMACHER, N., SCHWARZ, J., TANGERMANN, S., KENNER, L., SCHLEDERER, M., SIBILIA, M., LINDER, M., ALTENDORF-HOFMANN, A., KNOSEL, T., GRUBER, E. S., OBERHUBER, G., BOLIK, J., REHMAN, A., SINHA, A., LOKAU, J., ARNOLD, P., CABRON, A. S., ZUNKE, F., BECKER-PAULY, C., PREAUDET, A., NGUYEN, P., HUYNH, J., AFSHAR-STERLE, S., CHAND, A. L., WESTERMANN, J., DEMPSEY, P. J., GARBERS, C., SCHMIDT-ARRAS, D., ROSENSTIEL, P., PUTOCZKI, T., ERNST, M. & ROSE-JOHN, S. 2018. ADAM17 is

911 required for EGF-R-induced intestinal tumors via IL-6 trans-signaling. *J Exp Med*,
 912 215, 1205-1225.
 913 SIGGS, O. M., GRIEVE, A., XU, H., BAMBROUGH, P., CHRISTOVA, Y. & FREEMAN, M.
 914 2014. Genetic interaction implicates iRhom2 in the regulation of EGF receptor
 915 signalling in mice. *Biol Open*, 3, 1151-7.
 916 TYANOVA, S., TEMU, T., SINITCYN, P., CARLSON, A., HEIN, M. Y., GEIGER, T., MANN,
 917 M. & COX, J. 2016. The Perseus computational platform for comprehensive analysis
 918 of (prote)omics data. *Nat Methods*, 13, 731-40.
 919 VAN WILGENBURG, B., BROWNE, C., VOWLES, J. & COWLEY, S. A. 2013. Efficient, long
 920 term production of monocyte-derived macrophages from human pluripotent stem cells
 921 under partly-defined and fully-defined conditions. *PLoS One*, 8, e71098.
 922 YAMAMOTO, K., TRAD, A., BAUMGART, A., HUSKE, L., LORENZEN, I., CHALARIS, A.,
 923 GROTZINGER, J., DECHOW, T., SCHELLER, J. & ROSE-JOHN, S. 2012. A novel
 924 bispecific single-chain antibody for ADAM17 and CD3 induces T-cell-mediated lysis
 925 of prostate cancer cells. *Biochem J*, 445, 135-44.
 926 ZUNKE, F. & ROSE-JOHN, S. 2017. The shedding protease ADAM17: Physiology and
 927 pathophysiology. *Biochim Biophys Acta*.

928

Figures

Figure 1 - FRMD8 is a novel interaction partner of iRhom1 and iRhom2.

A Volcano plot representing results from three iRhom2 co-immunoprecipitations. The fold change of label-free quantification values (in log₂ ratio) was plotted against the p value (-log₁₀ transformed). The grey dotted line indicates p-values < 0.05 (analysed with a two-sample t-test). Benjamini-Hochberg correction was applied to adjust the p-value for multiple hypothesis testing (dark grey dotted line).

B Lysates of HEK293T cells stably expressing human iRhom1-3xHA or iRhom2-3xHA transfected with human FRMD8-V5 (where indicated) were subjected to anti-HA and anti-V5 immunoprecipitation (HA-IP, V5-IP) and a western blot using anti-HA and anti-V5 antibodies was performed. Black arrowheads indicated the co-immunoprecipitated FRMD8-V5; white arrowheads indicated the co-immunoprecipitated iRhoms.

Figure 2 - FRMD8 loss reduces mature ADAM17 levels and impairs ADAM17-dependent shedding activity.

A ADAM17 levels were analysed in HEK293T cells transfected with non-targeting siRNA control pool (ctrl) or FRMD8 SMARTpool siRNA after western blotting with anti-ADAM17 and anti-actin staining. In this and subsequent figures, pro- and mature form of ADAM17 are indicated with black and white arrowheads, respectively. Lower panel: Knockdown efficiency of FRMD8 was analysed by TaqMan PCR.

B, C Lysates from wild-type (WT) and FRMD8 knockout (KO) HEK293T cells, transiently transfected with FRMD8-V5 for 72 h (where indicated) and immunoblotted for endogenous ADAM17, ADAM10, FRMD8 and actin using western blotting. Nonspecific bands are marked with an asterisk.

D Cell surface levels of endogenous ADAM10 and ADAM17 were analysed in WT and FRMD8 KO HEK293T cells after stimulation with 200 nM PMA for 5 min. Unpermeabilised cells were stained on ice with ADAM10 and ADAM17 antibodies, or only with the secondary antibody as a control (grey). The immunostaining was analysed by flow cytometry. The graph shown is one representative experiment out of four biological replicates. The geometric mean fluorescence was calculated for each experiment using FlowJo software. Statistical analysis was performed using an unpaired t-test.

E, F WT and FRMD8 KO HEK293T cells were transiently transfected with alkaline phosphatase (AP)-tagged AREG, HB-EGF or TGF α , and then either incubated with 200 nM PMA, with 200 nM PMA and 1 μ M GW (ADAM10/ADAM17 inhibitor), or with DMSO for 30 min. In addition, cells transfected with AP-TGF α were either left unstimulated for 20 h or incubated with GW for 20 h. AP activity was measured in supernatants and cell lysates. Each

experiment was performed in biological triplicates. The results of three independent shedding experiments are shown. Statistical analysis was performed of using a Mann-Whitney test. ns = p-value > 0.05; * = p-value < 0.05; *** = p-value < 0.001; **** = p-value < 0.0001.

Figure 3 - FRMD8 binds to the iRhom2 N-terminus.

A Schematic representation of truncated human and mouse iRhom2 constructs used in (B-E).

B, C Lysates and anti-HA immunoprecipitation (HA-IP) from HEK293T cells transiently co-transfected with FRMD8-V5 and either empty vector (vect) or truncated human iRhom2-3xHA constructs were immunoblotted for V5 and HA.

D iRhom1/2 double knockout HEK293T cells stably expressing empty vector (vect) or human iRhom2-3xHA constructs were transiently transfected with alkaline phosphatase (AP)-tagged AREG and then incubated with 200 nM PMA or with DMSO for 30 min. AP activity was measured in supernatants and cell lysates. Each experiment was performed in biological triplicates. The results of three independent shedding experiments are shown. Statistical analysis was performed of using a Mann-Whitney test. **** = p-value < 0.0001.

E Lysates iRhom1/2 double knockout HEK293T cells transiently transfected with empty vector (vect) or human iRhom2-3xHA constructs were immunoblotted for ADAM17 and HA.

Figure 4 - iRhom2 binds to FRMD8 and ADAM17 simultaneously.

A Lysates, anti-HA and anti-V5 immunoprecipitations (HA-IP, V5-IP) of HEK293T cells co-expressing human iRhom2-3xHA and human FRMD8-V5 were immunoblotted for ADAM17, HA and V5.

B Lysates of wild-type (WT) and ADAM17 knockout (KO) HEK293T cells were transiently transfected with human iRhom2-3xHA and FRMD8-V5 (where indicated), anti-HA and anti-V5 immunoprecipitated (HA-IP; V5-IP) and immunoblotted for ADAM17, HA, and V5.

C Lysates of WT and FRMD8 KO HEK293T cells stably expressing human iRhom2-3xHA were anti-HA immunoprecipitated (HA-IP) and stained for ADAM17 and HA. Nonspecific bands are indicated by an asterisk.

D Lysates of WT and iRhom1/2 double knockout (DKO) HEK293T cells stably expressing human iRhom2^{WT}-3xHA or iRhom2^{Δ2001-300}-3xHA were anti-V5 immunoprecipitated (V5-IP) and immunoblotted for ADAM17, HA and V5.

Figure 5 - FRMD8 promotes cell surface localisation of iRhom2.

A, B Immunofluorescence of iRhom1/2 double knockout HEK293T cells stably expressing iRhom2-3xHA or iRhom2^{Δ300}-3xHA and transiently transfected with FRMD8-V5 for 72 h. Cells

were stained for HA (red), V5 (green) and DAPI for DNA (blue). Single confocal sections are shown, taken through the centre of the nucleus.

C Schematic model of the FRMD8-iRhom2^{Δ300} construct used in (E).

D, E Immunofluorescence of iRhom1/2 double knockout HEK293T cells stably expressing iRhom2^{Δ300}-3xHA or FRMD8-iRhom2^{Δ300}-3xHA and transiently transfected with ADAM17-V5 for 72 h. Cells were stained for HA (green), V5 (red) and DAPI for DNA (blue). Single confocal sections are shown, taken either through the centre of the nucleus (MEDIAL), or at basal regions close to the coverslip (BASAL). In all images the scale bar = 10 μm.

Figure 6 - FRMD8 loss leads to degradation of iRhoms and mature ADAM17 through the lysosomal pathway

A-D Immunofluorescence of iRhom1/2 double knockout HEK293T cells stably expressing iRhom2-3xHA or iRhom2^{Δ300}-3xHA treated with DMSO (CON) or 100 nM bafilomycin A1 (BAF) for 16 h prior to fixation. Cells were stained for HA (green), the lysosomal marker LAMP1 (red) and DAPI for DNA (blue). LAMP1-labelled regions (within white boxes) have been magnified. Scale bar = 10 μm.

E, F iRhom2^{Δ300}-3xHA cells were treated as in (A-D), but with 72 h expression of ADAM17-V5 and labelling of HA (green), V5 (red) and DAPI for DNA (blue). Arrows indicate colocalising puncta. Single confocal sections are shown, taken through the centre of the nucleus. HA- and V5-labelled regions (within white boxes) have been magnified. Scale bar = 10 μm

G Cell lysates of wild-type (WT) and FRMD8 knockout (KO) HEK293T cells treated with the solvent DMSO (–), 10 μM MG-132 (MG) or 200 nM bafilomycin A1 (Baf) for 16 h were enriched for glycosylated proteins using concanavalin A (conA) beads and immunoblotted for ADAM17 and transferrin receptor 1 (TfR). TfR was used as a loading control although it is also susceptible to bafilomycin treatment. Mature ADAM17 levels from three experiments were quantified relative to TfR levels using ImageJ.

Figure 7 - FRMD8 loss leads to the destabilisation of ADAM17 and iRhom2.

A Unpermeabilised WT (black) and FRMD8 KO HEK293T (red) cells stably expressing human iRhom2-3xHA were immunostained on ice for HA. Wild-type HEK293T cells immunostained for HA served as a negative control (grey).

B Cells were permeabilised and stained at room temperature with an anti-HA antibody. Immunostaining with the Alexa Fluor 488-coupled secondary antibody served as a control (grey). In (B & C), the flow cytometry graphs shown are one representative experiment out of three experiments. The geometric mean fluorescence was calculated for each experiment

using FlowJo software. Statistical analysis was performed using an unpaired t-test; ns = p-value > 0.05; * = p-value < 0.05.

C Lysates of HEK293T cells stably expressing human iRhom2-3xHA and transiently transfected with FRMD8-V5 (where indicated) were analysed by western blot for iRhom2 levels using anti-HA, anti-V5 and anti-actin immunostaining. Nonspecific bands are marked with an asterisk.

D Lysates of WT and FRMD8 KO HEK293T cells stably expressing human iRhom2-3xHA (where indicated) were immunoblotted for HA, FRMD8 and actin. An asterisk marks nonspecific bands.

E FRMD8 mRNA levels relative to actin mRNA levels were determined by TaqMan PCR in cells used in (D).

Figure 8 - FRMD8 stabilises endogenous iRhom2.

A, B Levels of endogenously 3xHA tagged iRhom2 were analysed in HEK293T-iRhom2-3xHA cells transfected with FRMD8-V5 plasmid, siRNAs targeting iRhom2, non-targeting siRNA control pool (ctrl) or FRMD8 SMARTpool siRNA. Cell lysates were anti-HA immunoprecipitated (HA-IP) to detect endogenous iRhom2-3xHA levels and immunoblotted using anti-HA antibody. Cell lysates were immunoblotted for ADAM17, V5, and actin.

C FRMD8 and iRhom2 mRNA levels relative to actin mRNA levels were determined by TaqMan PCR in cells used for the experiment shown in (B) to demonstrate that the destabilisation of endogenous iRhom2 was not induced by a change in iRhom2 mRNA levels.

Figure 9 - FRMD8 is required for TNF α release in human iPSC-derived macrophages.

A Schematic representation of the differentiation protocol of iPSCs into macrophages based on (van Wilgenburg et al., 2013). Scale bars = 10 μ m.

B Lysates of iPSC-derived macrophages (on day 7 after harvest from EBs) were immunoblotted for ADAM17, FRMD8, and actin. Western blots from three experiments were quantified using ImageJ with actin serving as the loading control.

C 25,000 iPSC-derived macrophages were either left unstimulated, stimulated with 50 ng/ml LPS for 4 h. TNF α concentration in the cell supernatants was measured by ELISA and then normalised to the protein concentration in macrophage cell lysates to adjust the cytokine release for potential differences in cell numbers. Each experiment was performed in biological triplicates. Data from three independent experiments were statistically analysed using a Mann-Whitney test; *** = p-value < 0.001; **** = p-value < 0.0001.

D, E Lysates from tissues derived from *Frmd8*^{-/-} or *Rhbd2*^{-/-} and their wild-type littermates were immunoblotted for ADAM17, FRMD8, iRhom2 and actin. Blots from three experiments

1075 using three different sets of *Frmd8*^{-/-} and *Frmd8*^{+/+} mice were quantified using ImageJ with
1076 actin serving as the loading control.

1077

1078 **Figure 10 - FRMD8 stabilises the iRhom2/ADAM17 sheddase complex at the cell**
1079 **surface.**

1080 Schematic representation of the role of FRMD8 in the iRhom2/ADAM17 pathway: under wild-
1081 type conditions ADAM17 and iRhom2 are stabilised by FRMD8 and thereby protected from
1082 degradation through the endolysosomal pathway.

1083

1084

Tables

Table 1 - List of iRhom2 interaction partners identified in the mass spectrometry screen that have either shown a significant adjusted p-value or been reported previously (Adrain et al., 2012, McIlwain et al., 2012, Grieve et al., 2017). P-values from a two-sample t-test in Perseus are listed below (p-values > 0.05 written in grey). P-values were adjusted for multiple hypothesis testing with the Benjamini-Hochberg correction and are listed under “adjusted p-values” (p-values > 0.05 written in grey).

Prot. ID	Protein name	Gene	p-value	adjusted p-value
Q9BZ67	FERM domain-containing protein 8	FRMD8	$2.44 \cdot 10^{-7}$	$2.38 \cdot 10^{-4}$
Q9BY50	Signal peptidase subunit SEC11C	SEC11C	$2.94 \cdot 10^{-6}$	$1.71 \cdot 10^{-3}$
Q9NUP9	Protein lin-7 homolog C	LIN7C	$1.55 \cdot 10^{-5}$	$6.45 \cdot 10^{-3}$
P11940	Polyadenylate-binding protein 1; Polyadenylate-binding protein 3	PABPC1; PABPC3	$2.10 \cdot 10^{-5}$	$7.66 \cdot 10^{-3}$
Q9BXB1	Leucine-rich repeat-containing GPCR 4	LGR4	$2.63 \cdot 10^{-5}$	$8.53 \cdot 10^{-3}$
O00629	Importin subunit alpha-3	KPNA4	$5.76 \cdot 10^{-5}$	$1.40 \cdot 10^{-2}$
Q13454	Tumor suppressor candidate 3	TUSC3	$7.05 \cdot 10^{-5}$	$1.58 \cdot 10^{-2}$
Q9HD26	GOPC/PIST	GOPC	$8.54 \cdot 10^{-5}$	$1.78 \cdot 10^{-2}$
Q9UKX7	Nuclear pore complex protein Nup50	NUP50	$8.77 \cdot 10^{-5}$	$1.71 \cdot 10^{-2}$
O95754	Semaphorin-4F	SEMA4F	$1.06 \cdot 10^{-4}$	$1.83 \cdot 10^{-2}$
Q96EK5	KIF1-binding protein	KIAA1279	$1.47 \cdot 10^{-4}$	$2.26 \cdot 10^{-2}$
P51809	Vesicle-associated membrane protein 7	VAMP7	$1.55 \cdot 10^{-4}$	$2.26 \cdot 10^{-2}$
Q12899	Tripartite motif-containing protein 26	TRIM26	$1.93 \cdot 10^{-4}$	$2.68 \cdot 10^{-2}$
O14763	TRAIL receptor 2	TNFRSF10B	$2.29 \cdot 10^{-4}$	$3.04 \cdot 10^{-2}$
Q5SWA1	Protein phosphatase 1 subunit 15B	PPP1R15B	$3.35 \cdot 10^{-4}$	$4.25 \cdot 10^{-2}$
Q6PJF5	iRhom2	RHBDF2	$3.42 \cdot 10^{-4}$	$4.16 \cdot 10^{-2}$
P61225	Ras-related protein Rap-2b	RAP2B	$4.27 \cdot 10^{-4}$	$4.98 \cdot 10^{-2}$
P28482	Mitogen-activated protein kinase 1	MAPK1	$3.37 \cdot 10^{-3}$	0.22
P27361	Mitogen-activated protein kinase 3	MAPK3	$5.34 \cdot 10^{-3}$	0.32
P62258	14-3-3 protein epsilon	YWHAE	$6.61 \cdot 10^{-3}$	0.35
P78536	ADAM17	ADAM17	$8.07 \cdot 10^{-3}$	0.40
P63104	14-3-3 protein zeta/delta	YWHAZ	$9.14 \cdot 10^{-3}$	0.41
P27348	14-3-3 protein theta	YWHAQ	$1.20 \cdot 10^{-2}$	0.45

P31947	14-3-3 protein sigma	SFN	$2.19 \cdot 10^{-2}$	0.63
Q04917	14-3-3 protein eta	YWHAH	$2.33 \cdot 10^{-2}$	0.65
P61981	14-3-3 protein gamma	YWHAG	$3.15 \cdot 10^{-2}$	0.75
P31946	14-3-3 protein alpha/beta	YWHAB	$6.53 \cdot 10^{-2}$	1
P51812	Ribosomal protein S6 kinase alpha-3	RPS6KA3	$6.53 \cdot 10^{-2}$	1

1093

Supplementary figures

Figure 1-figure supplement 1

A HEK293T cells transiently transfected with human iRhom2-3xHA or UNC93B1-3xHA were stained with DAPI (blue) to label nuclei, anti-HA to label iRhom2-HA (red), and anti-calnexin to label the ER (green). Scale bar = 10 μ m.

B Lysates and anti-HA immunoprecipitation (HA-IP) from wild-type (WT) and FRMD8 knockout (KO) HEK293T cells stably expressing iRhom2-3xHA (indicated) were immunoblotted for HA and FRMD8. Nonspecific bands are marked with an asterisk.

Figure 3-figure supplement 1

A Amino acid sequence alignment of human and mouse iRhom2 N-terminal region using Clustal Omega. The region required for FRMD8 binding is highlighted in red. Conserved phosphorylation sites that have been mutated to alanine in the iRhom2^{pDEAD} (Figure 3E) are marked in yellow. Grey residues indicate additional phosphorylation sites that have been reported on PhosphoSitePlus (www.phosphosite.org). An asterisk (*) indicates positions which have a fully conserved residue, a colon (:) indicates strongly similar properties of the amino acids, and a period (.) indicates weakly similar properties according to the Clustal Omega tool.

B Lysates and anti-HA immunoprecipitation (HA-IP) from HEK293T cells transiently transfected with FRMD8-V5 and either empty vector (vect), mouse iRhom2^{WT} (WT) or Rhom2^{cub} (Δ 268) were immunoblotted for V5 and HA.

Figure 7-figure supplement 1

A iRhom1/2 double knockout HEK293T cells stably expressing iRhom2^{WT}-3xHA, iRhom2 ^{Δ 300}-3xHA or FRMD8-iRhom2 ^{Δ 300}-3xHA were treated with 100 μ g/ml cycloheximide for the indicated time (0-8 h) to block protein synthesis. Cell lysates were immunoblotted for HA and actin.

B Cell lysates of wild-type (WT) and FRMD8 knockout (KO) HEK293T cells treated with 10 μ M MG-132 (MG), 200 nM bafilomycin A1 (Baf) or 50 mM ammonium chloride (NH₄Cl) for 16 h were immunoblotted for ADAM17, FRMD8, and actin. An asterisk marks a nonspecific band.

C N-glycosylation of iRhom2 was analysed using EndoH and PNGase to distinguish ER/*cis*-Golgi (EndoH sensitive) and late Golgi localisation (EndoH resistant). Lysates of WT and FRMD8 KO HEK293T cells transiently transfected with mouse iRhom2-3xHA were deglycosylated with EndoH or PNGase and then immunoblotted for mouse iRhom2, human FRMD8 and actin. An asterisk marks a nonspecific band.

D Lysates of HEK293T cells stably expressing human iRhom1-3xHA and transfected with FRMD8-V5 (where indicated) were immunoblotted for HA, V5, and actin.

E Levels of ADAM17 were analysed in HEK293T-iRhom2-3xHA and HEK293T WT cells transfected with siRNAs targeting iRhom2 where indicated. Cell lysates were immunoblotted using an anti-ADAM17 or anti-actin antibody. An asterisk marks a nonspecific band.

Figure 9-figure supplement 1

A Sequencing of the genomic DNA isolated from clonal FRMD8 KO iPSCs shows a 1-nt insertion (clone 1) and a 7-nt and 10-nt deletion (clone 2). The targeting sequence of the sgRNA is shown in bold; small letters indicate the sequence within the intronic region; the protospacer adjacent motif (PAM) sequence underlined.

B Parental wild-type (left) and FRMD8 KO (right) iPSC lines were karyotyped by SNP array. Detected copy number variations are indicated in red (DNA copy number loss in the indicated region) and green (DNA copy number increase). The AH017-13 iPSC line used was derived from a female donor therefore the Y chromosome is marked in red (loss of Y chromosome DNA).

C 25,000 iPSC-derived macrophages were either left unstimulated, stimulated with 50 ng/ml LPS, or with 50 ng/ml LPS and simultaneously with 2 μ M GI or 2 μ M GW for 4 h. TNF α concentration in the cell supernatants was measured by ELISA and then normalised to the protein concentration in macrophage cell lysates to adjust the cytokine release for potential differences in cell numbers. Each experiment was performed in biological triplicates. Data from three independent experiments were statistically analysed using a Mann-Whitney test; ns = p-value > 0.05; **** = p-value < 0.0001.

D TNF α mRNA levels relative to actin mRNA levels were measured by TaqMan PCR in WT and FRMD8 KO iPSC-derived macrophages without stimulation and after stimulation with 200 ng/ml LPS for 0.5 h.

Figure 9-figure supplement 2

A Schematic representation of the insertion of a lacZ/neomycin cassette into the *Frdm8* locus in the ES cells used to generate *Frdm8*^{-/-} mice.

B Off-spring of *Frdm8*^{+/-} x *Frdm8*^{+/-} (HET x HET) crosses listed by genotype: *Frdm8*^{+/+} (WT), *Frdm8*^{+/-} (HET), and *Frdm8*^{-/-} (KO). Two *Frdm8* mouse strains were bred (both in BL6 background): one with the entire lacZ/neomycin cassette inserted and one strain in which the neomycin resistance gene has been removed from the cassette.

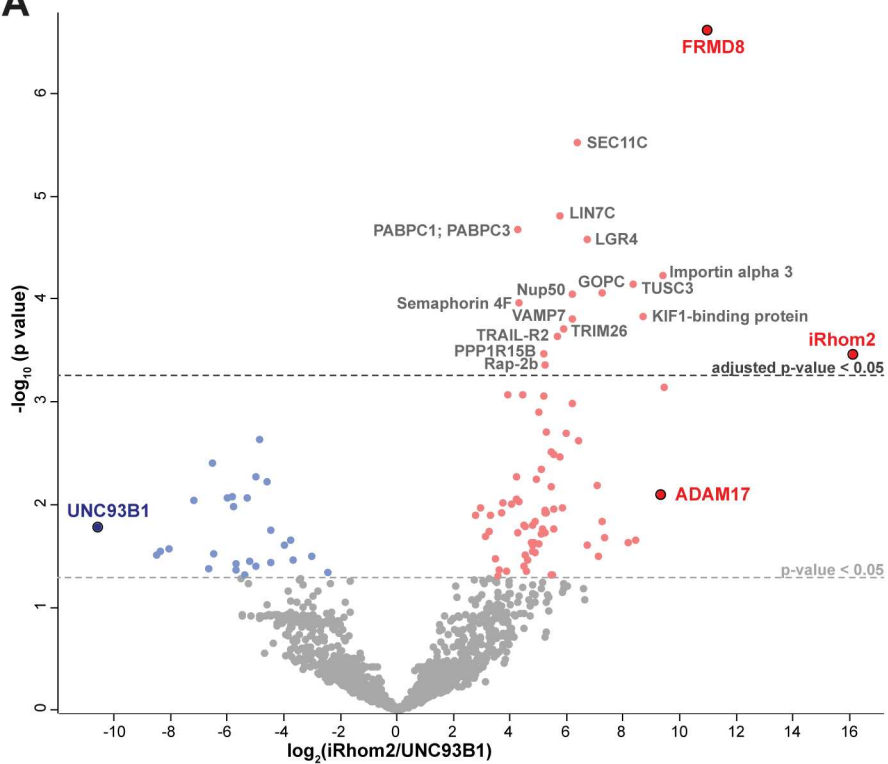
C Lysates from skin derived from *Frdm8*^{-/-}, *Rhbd12*^{-/-} mice and their wild-type littermate were immunoblotted for iRhom2 and actin.

1168 **Figure 10-figure supplement 1**

1169 Lysates and anti-HA immunoprecipitation (HA-IP) from HEK293T cells transiently transfected
1170 with human FRMD8-V5 and mouse iRhom2^{WT} (WT) or iRhom2^{pDEAD} (pDEAD) were
1171 immunoblotted for V5 and HA. Where indicated cells have been stimulated with 200 nM PMA
1172 for 30 min.

Figure 1

A



B

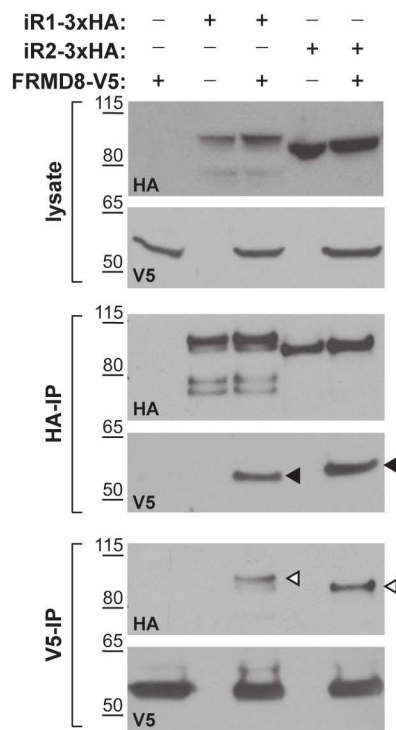


Figure 2

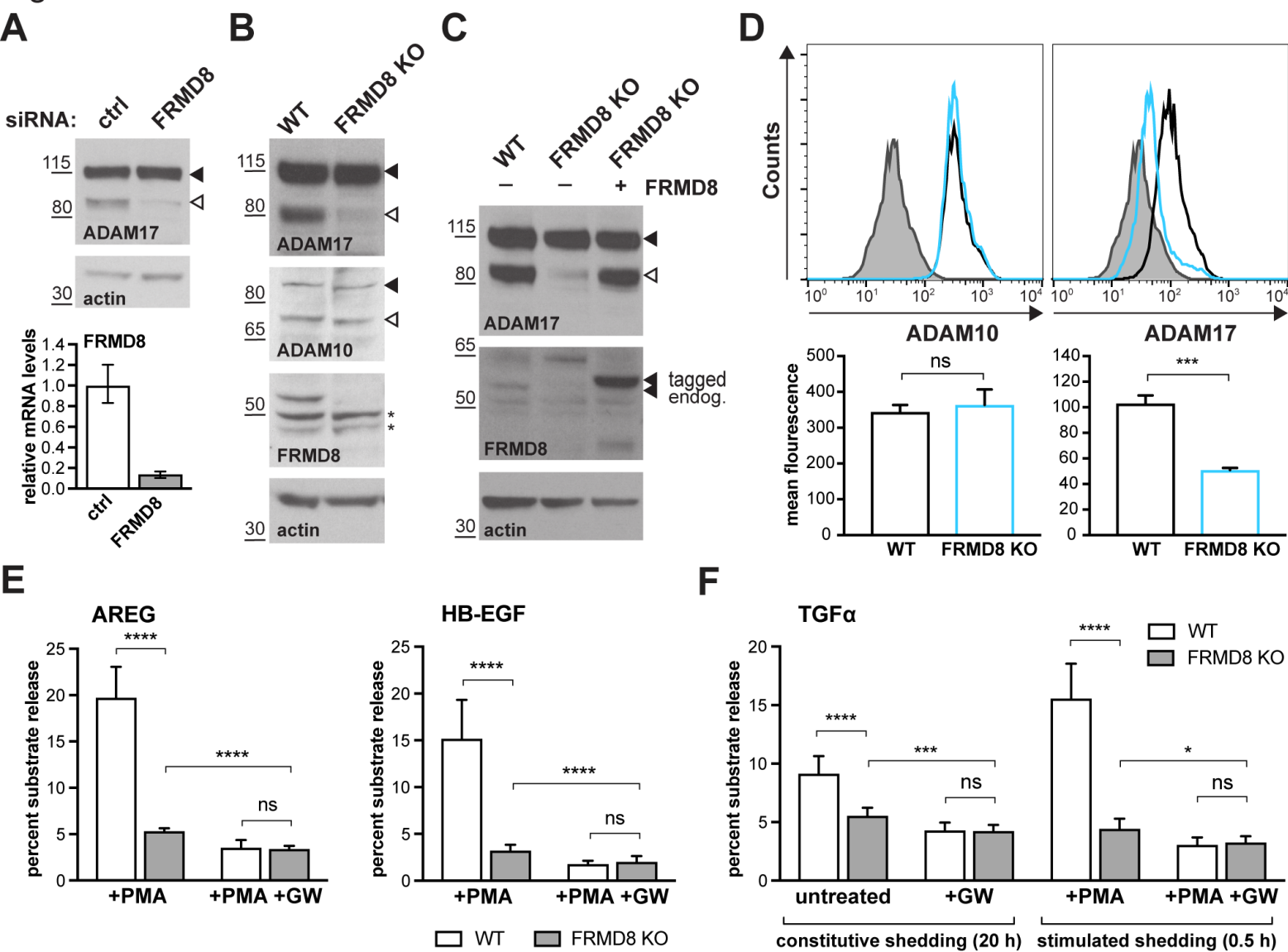
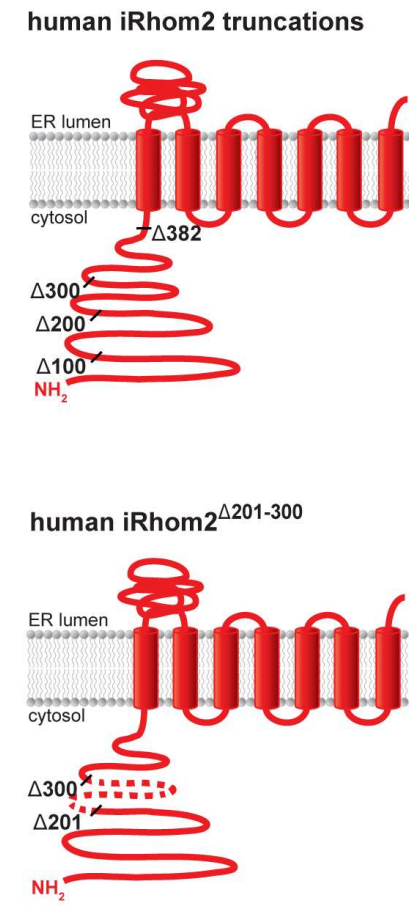
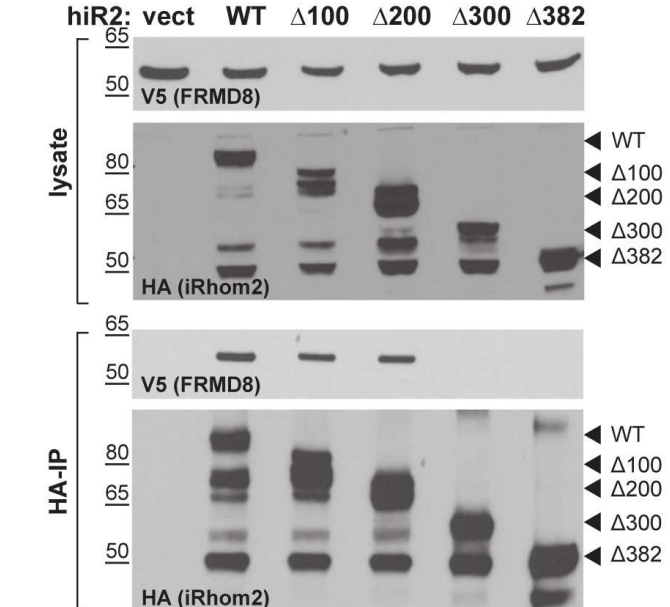


Figure 3

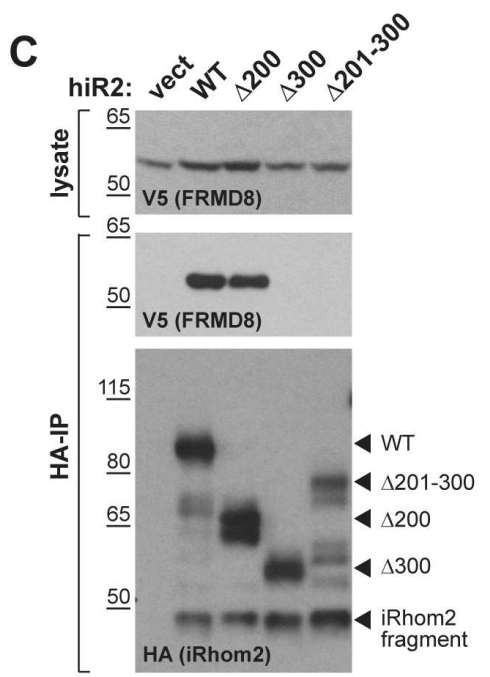
A



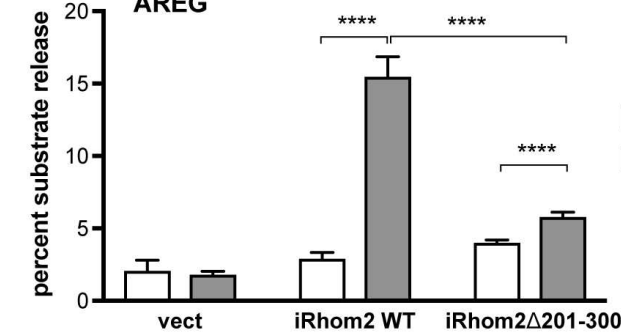
B



C



D



E

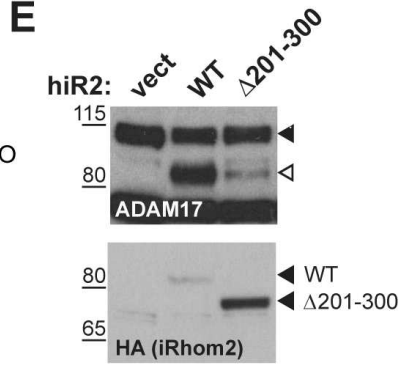
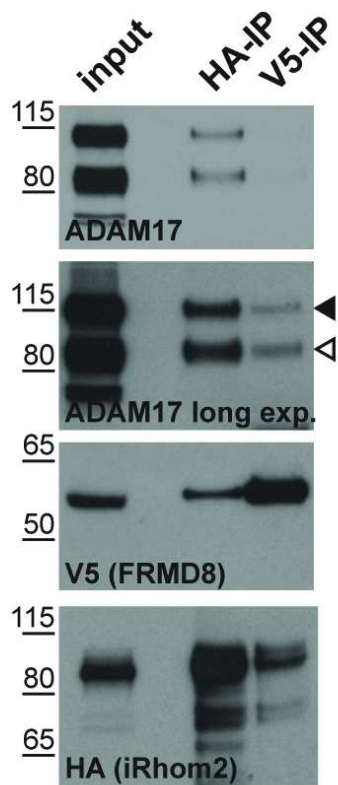
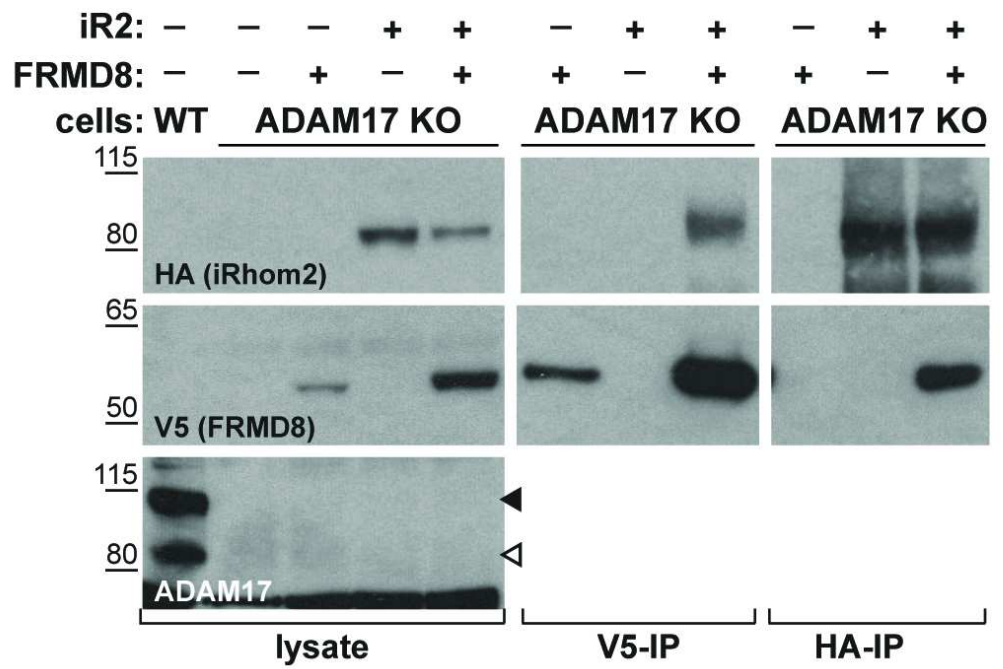


Figure 4

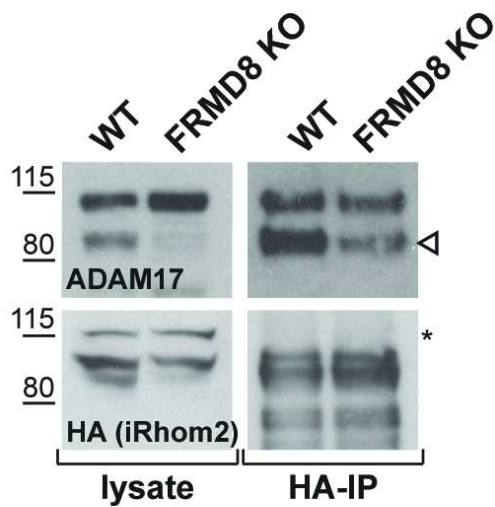
A



B



C



D

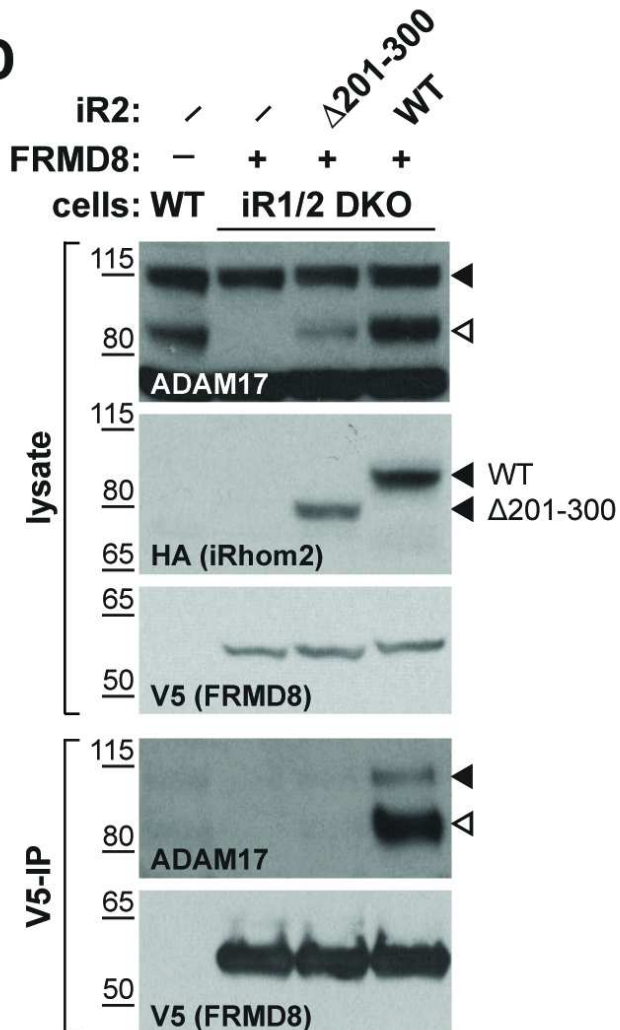
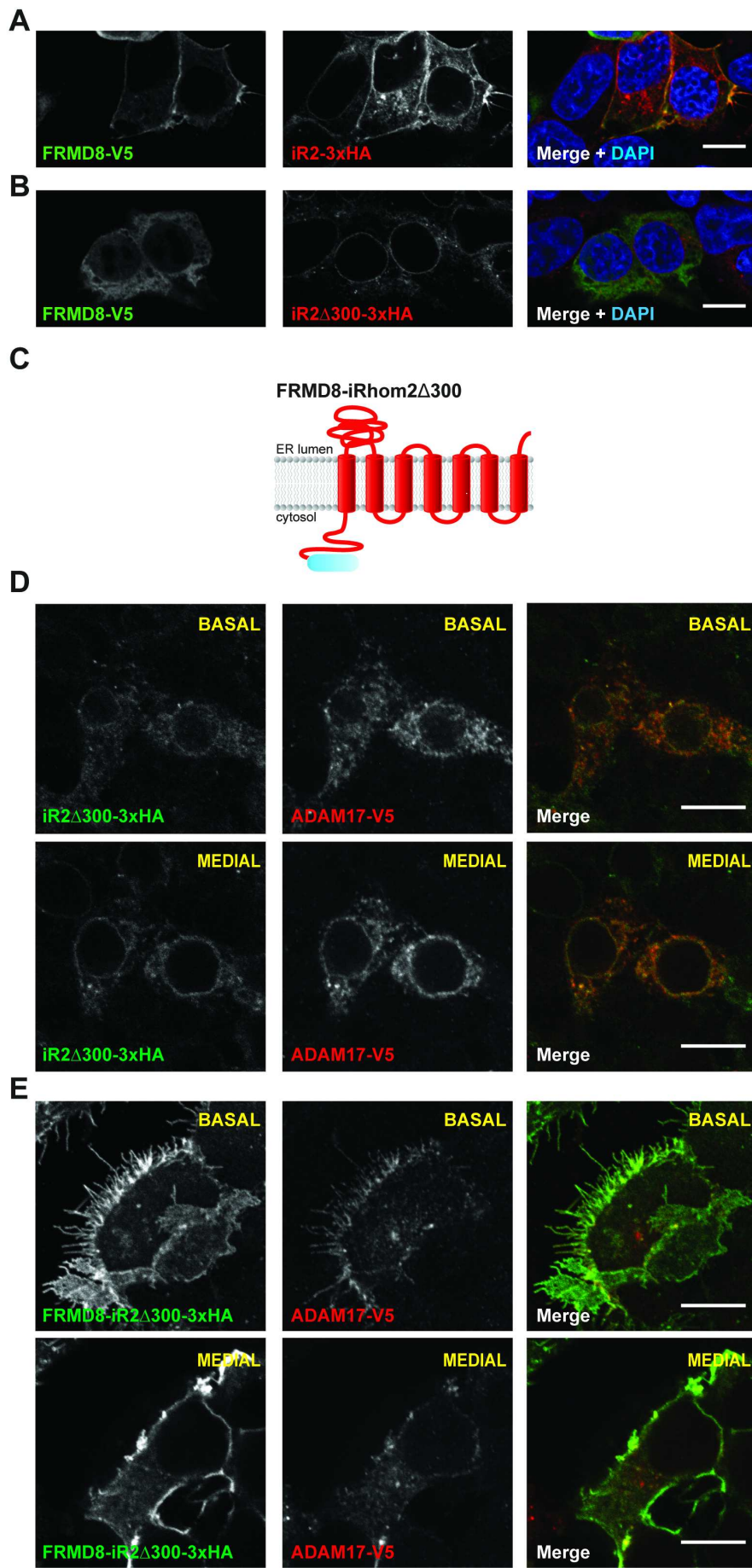
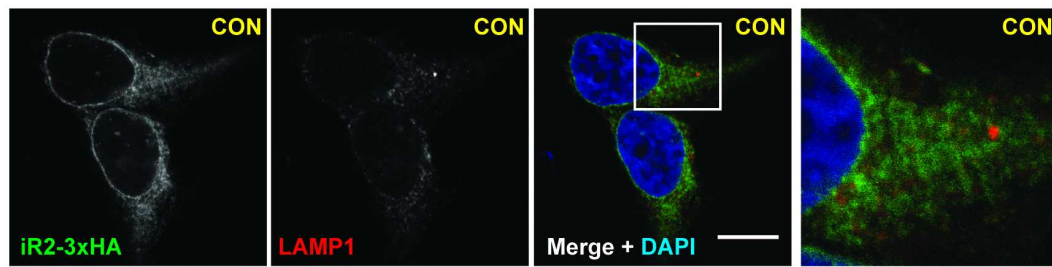


Figure 5

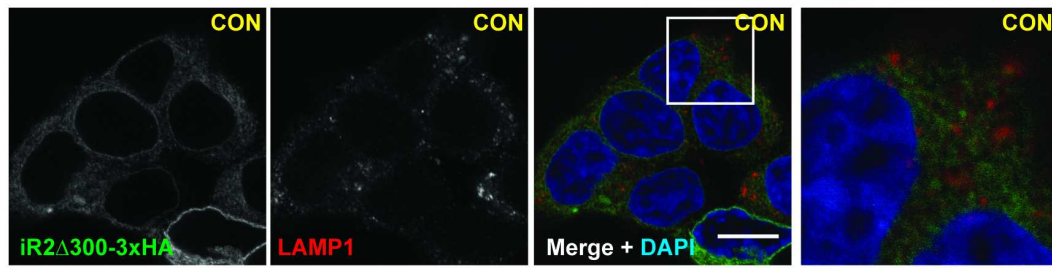


A

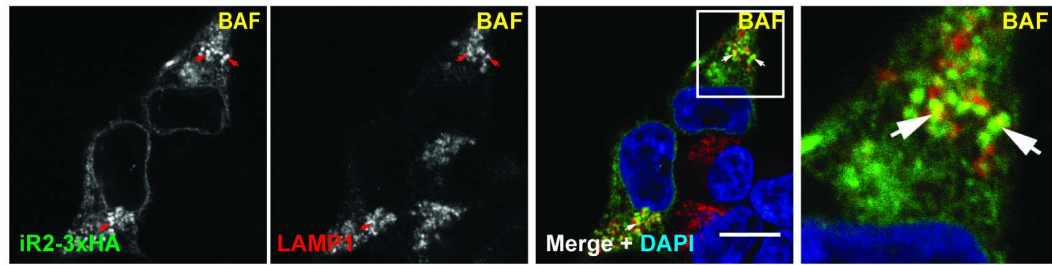
A



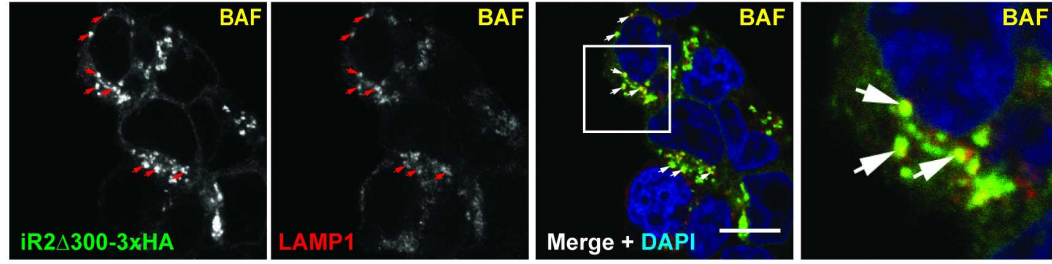
B



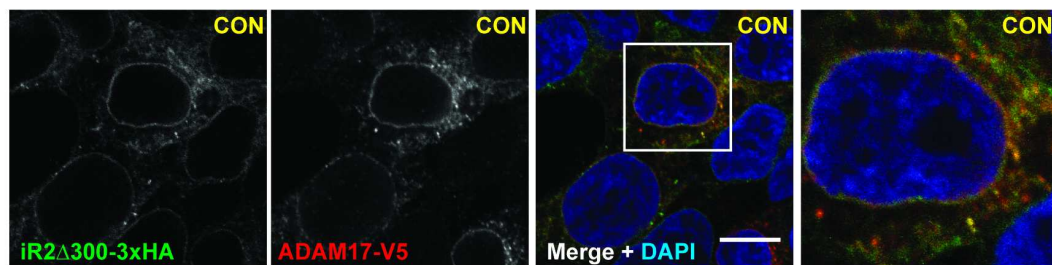
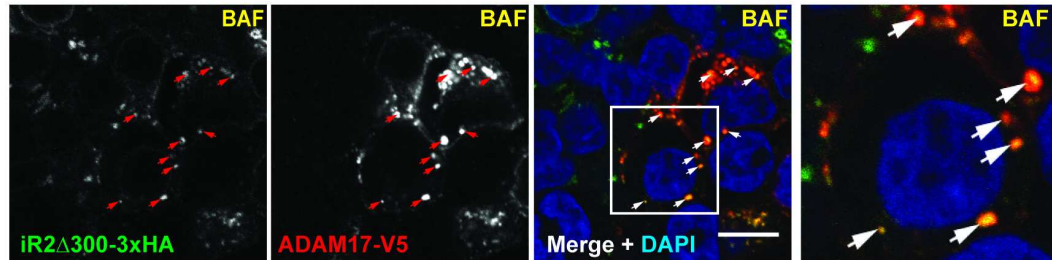
C



D



E

**F**

G

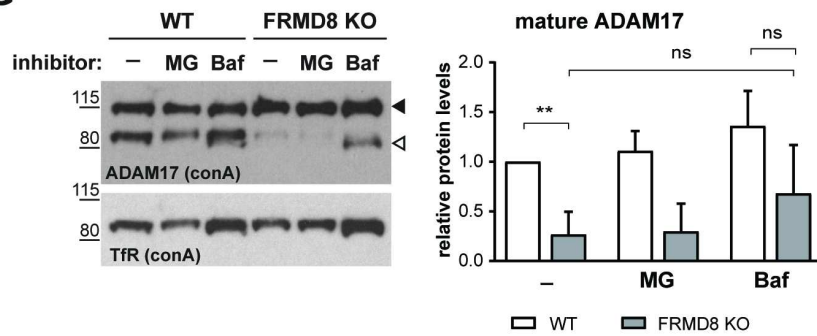


Figure 7

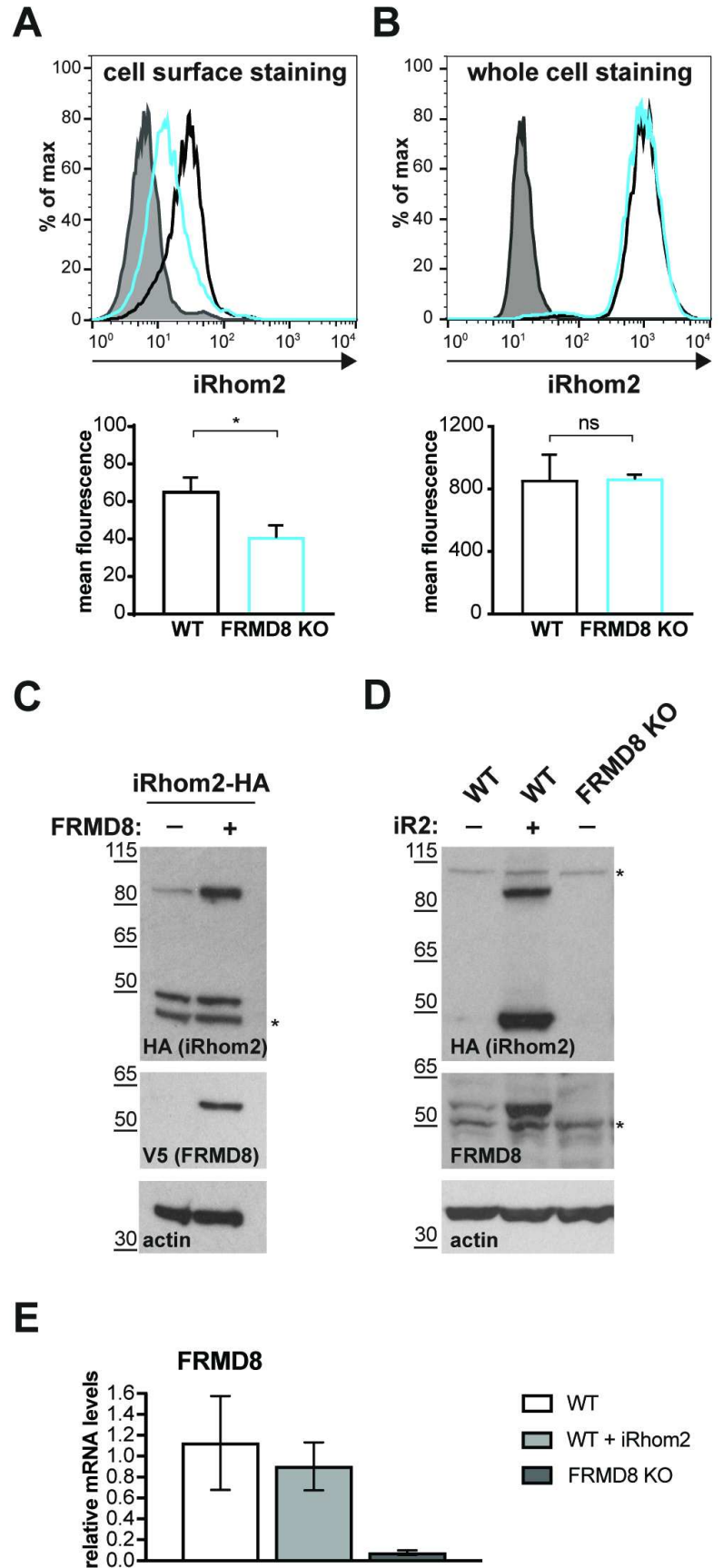
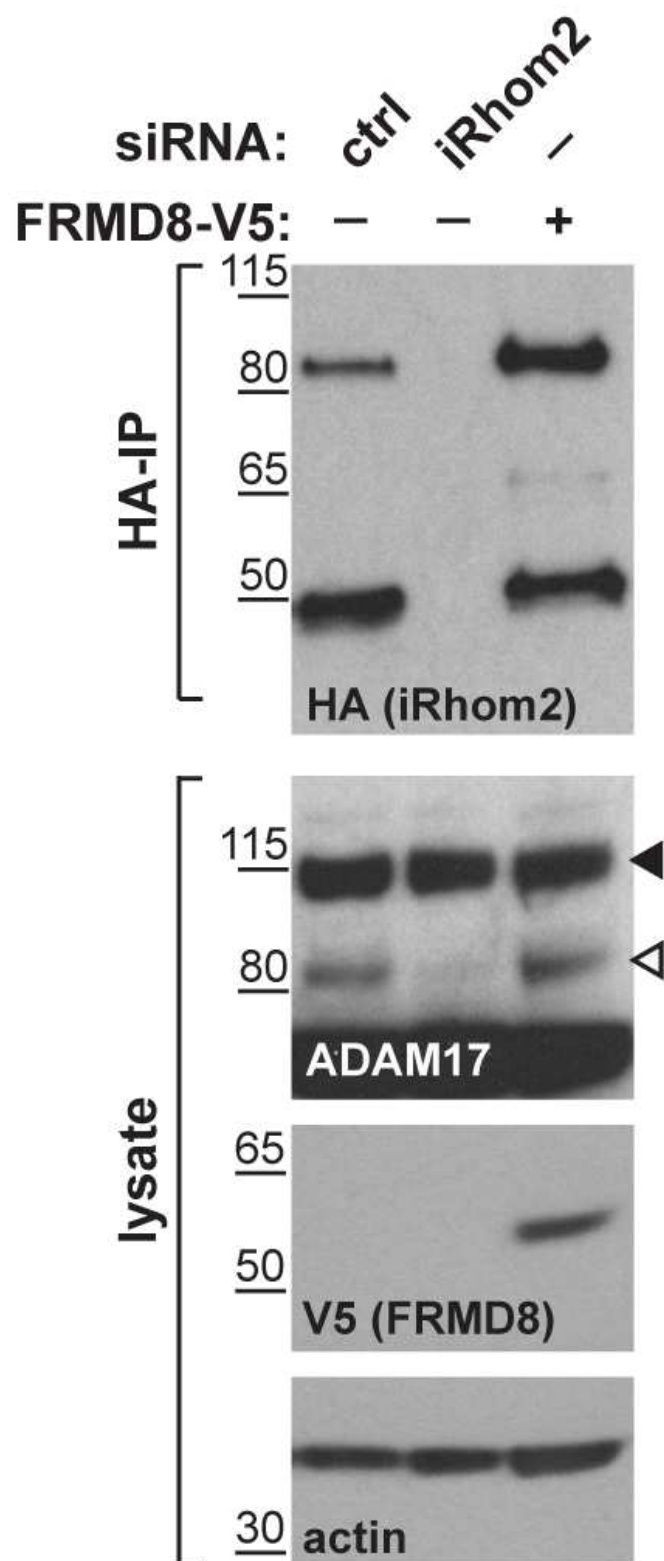
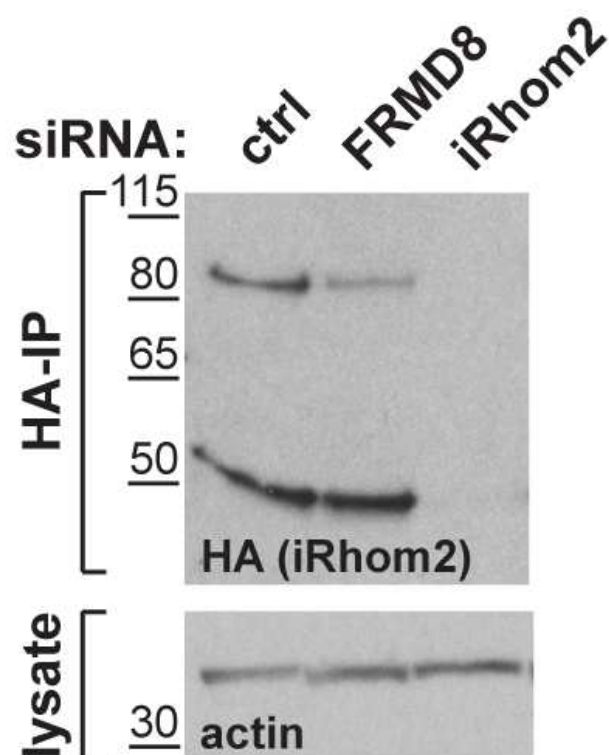


Figure 8

A



B



C

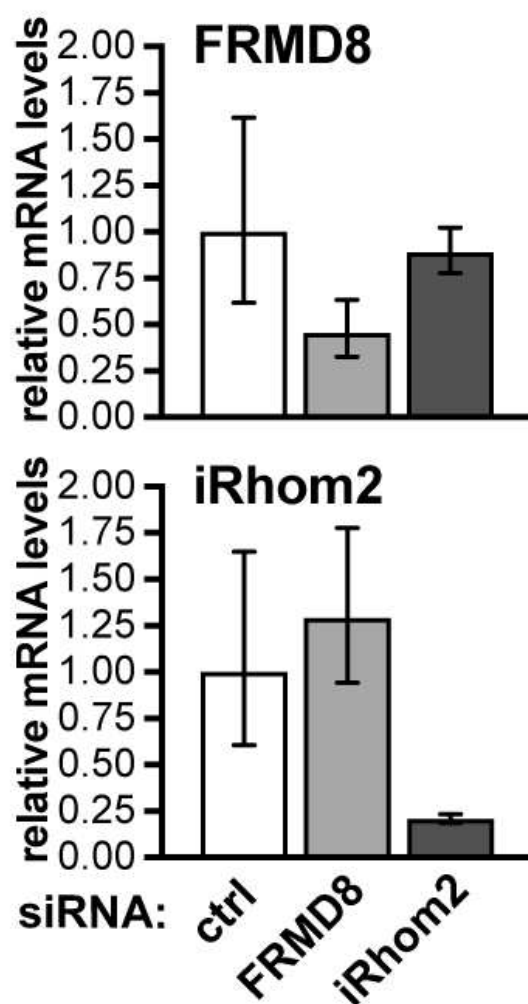
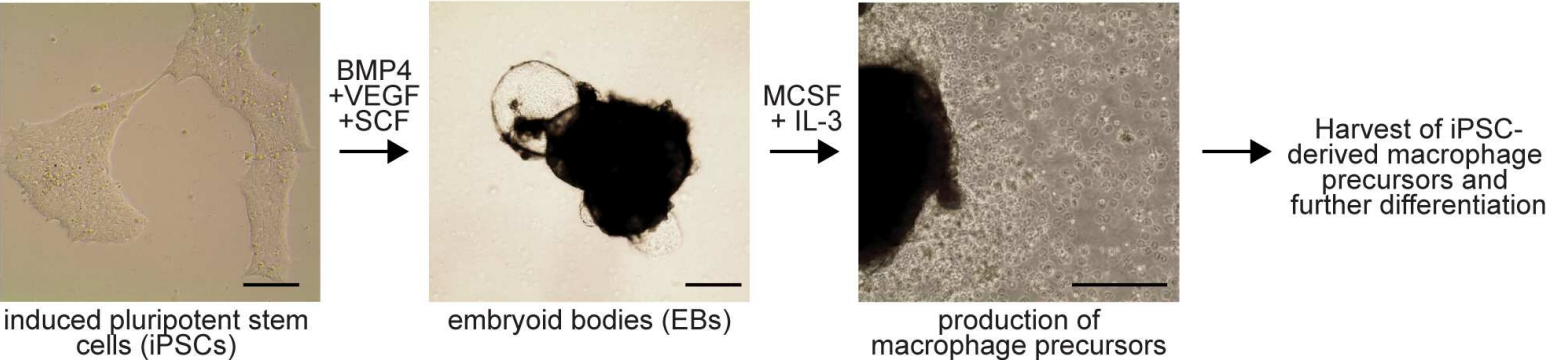
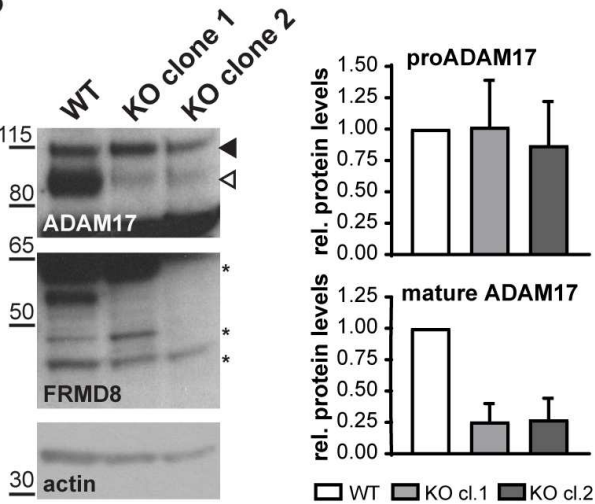


Figure 9

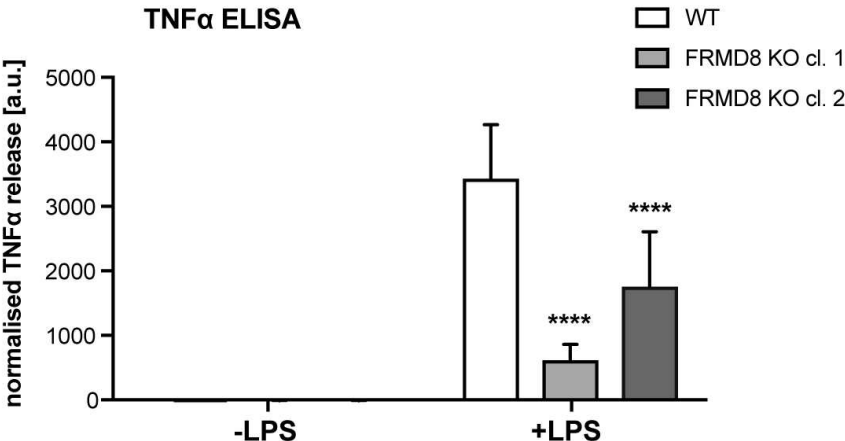
A



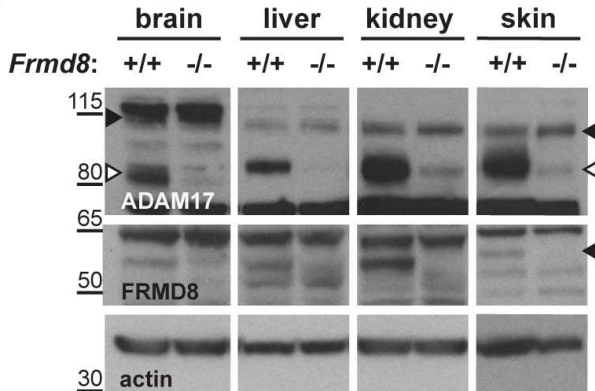
B



C



D



E

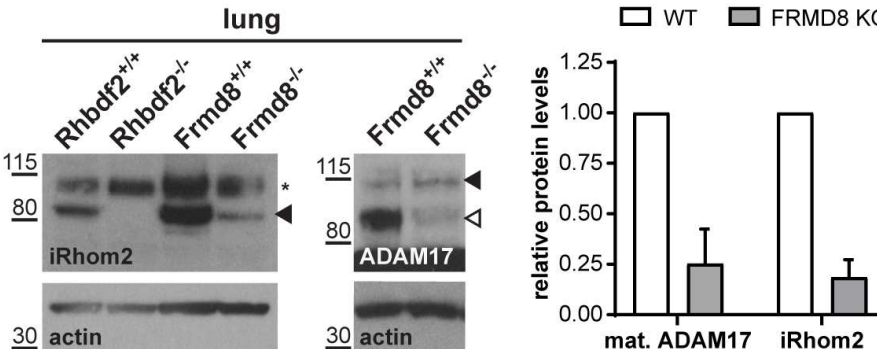
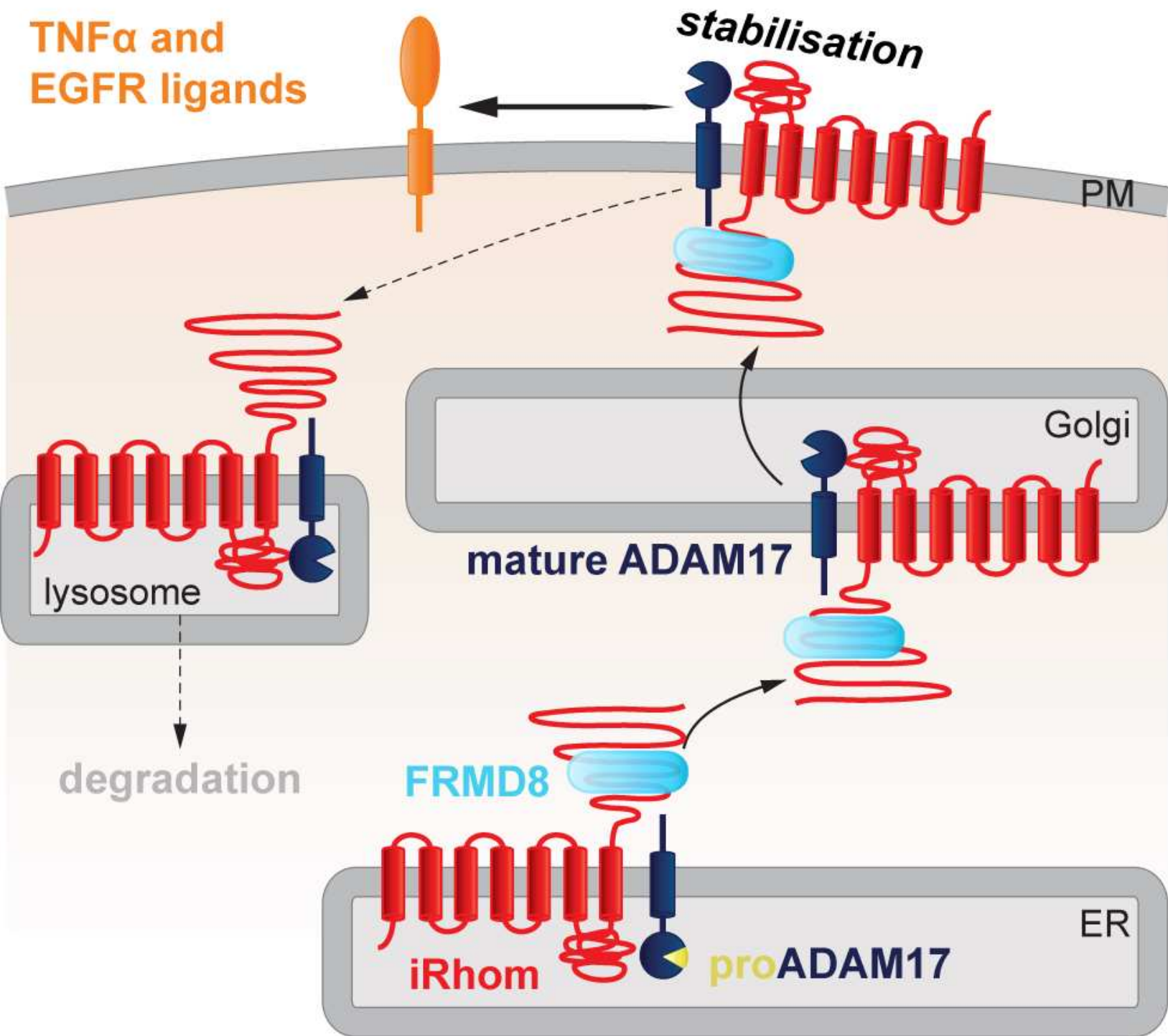
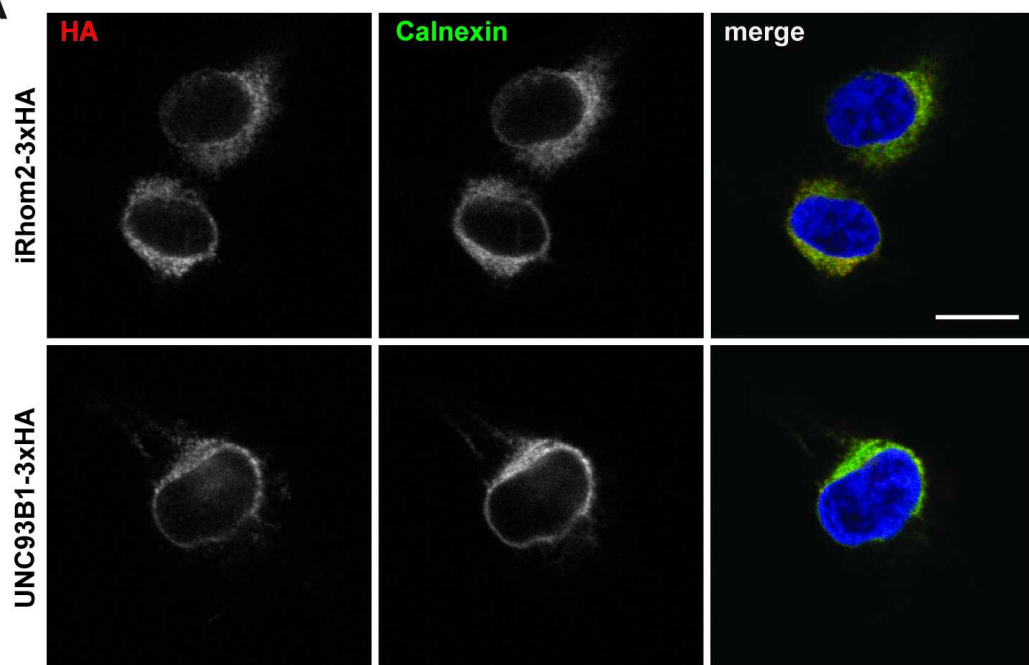
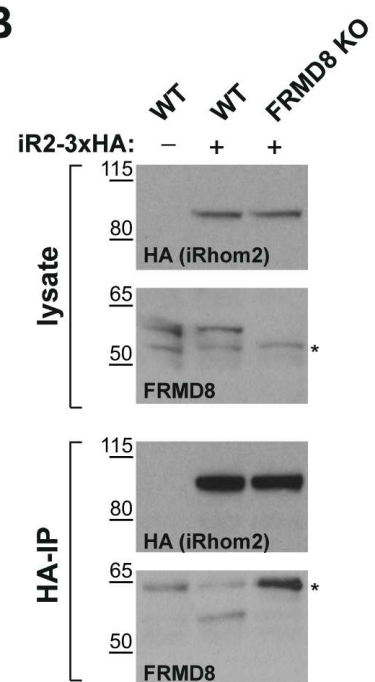


Figure 10

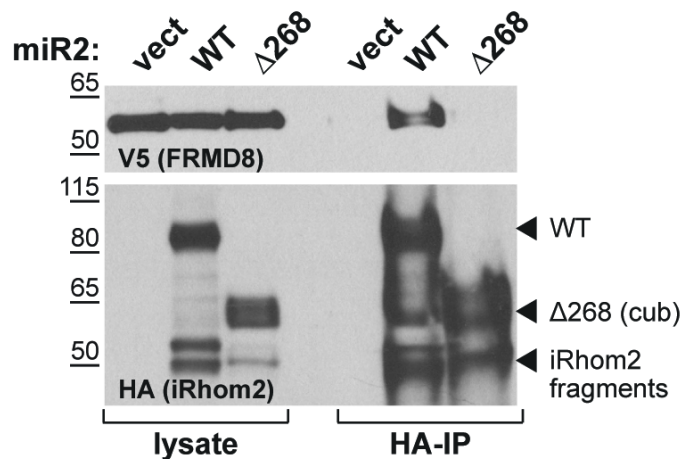


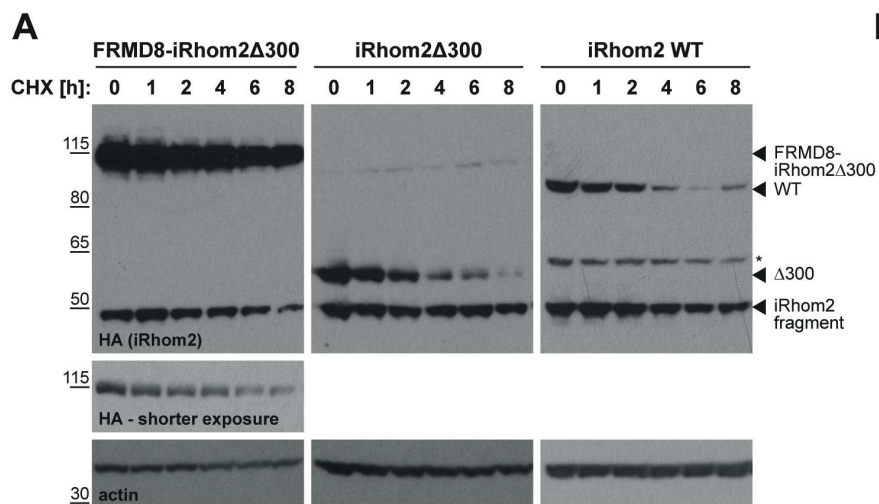
A**B**

A

human	MASADKNGGSVSSVSSSRLLQSRKPPNLSITIPPPEKETQAPGEQDSMLPEGFQNRRLKKS	60
mouse	MASADKNGSNLPSVSGSRLQSRKPPNLSITIPPPE--SQAPGEQDSMLPE-----	48
*****.:***.*****:*****		
Δ100		
human	QPRTWASHTTACPPSFLPKRKNPAYLKSVSLQEPRSRWQESSEKRPGRFRRQASLSQSIRK	120
mouse	-----RRKNPAYLKSVSLQEPRGRWQEGAERPGFRRQASLSQSIRK	90
:*****.***.:*****		
human	GAAQWFGVSGDWEGQRQQWQRRSLHHCSMRYGRLKASCQRDLELPSQEAPSFQGTESPKP	180
mouse	STAQWFGVSGDWEGKRQNWHRRLHHCSVHYGRLKASCQRELELPSQEVPSFQGTESPKP	150
.:*****:*.*:*****:*****:*****.*****		
Δ200		
human	CKMPKIVDPLARGRAFRHPEEMDRPHALHPPLTPGVLSLTSFTSVRSGYSHLPRRKRMVS	240
mouse	CKMPKIVDPLARGRAFRHPDEVDRPHAAHPPLTPGVLSLTSFTSVRSGYSHLPRRKRIISV	210
*****.:*****.*****.*****.*****.*****		
Δ300		
human	AHMSLQAAAALLKGRSVLDATGQRCRVVKRSFAFPSFLEEDVVDGADTFDSSFFSKEEMS	300
mouse	AHMSFQAAAALLKGRSVLDATGQRCRHVKRSFAYPSFLEEDAVDGADTFDSSFFSKEEMS	270
****.*****.*****.*****.*****.*****		
Δ268		
human	SMPDDVFESPPLSASYFRGIPHSA ^S SPVSPDGVQIPLKEYG--RAPVPGPRRGKRIASKVK	358
mouse	SMPDDVFESPPLSASYFRGVPHSA ^S SPVSPDGVHIPLKEYSGGRALGPGTQRGKRIASKVK	330
*****.*****.*****.*****.***.***.*****		
Δ382		
human	HFAFDRKKRHYGLGVGNWLNRSYRRSISSTVQRQLESFDSHRPYFTYWLT	409
mouse	HFAFDRKKRHYGLGVGNWLNRSYRRSISSTVQRQLESFDSHRPYFTYWLT	381

B





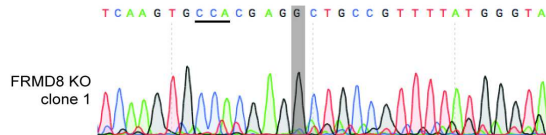
A

FRMD8 KO clone 1

WT
KO allele 1+2

PAM
CCACGAGCTGCCGTTTTATGGgt
CCACGAGCTGCCGTTTTATGGgt

exon 7'intron
1 nt insertion

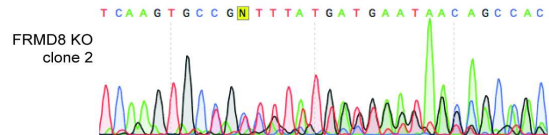


FRMD8 KO clone 2

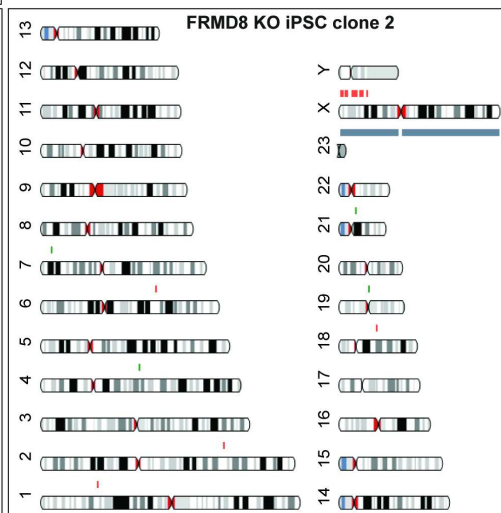
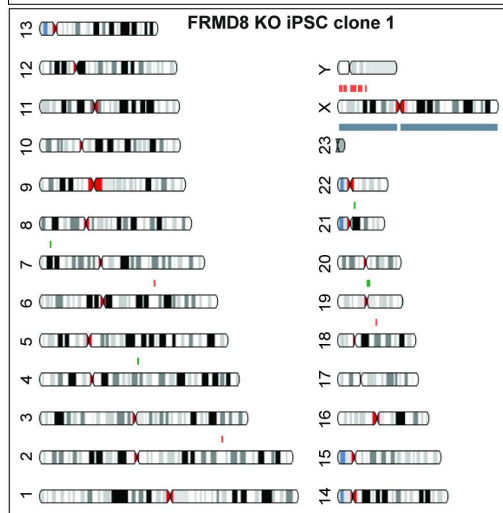
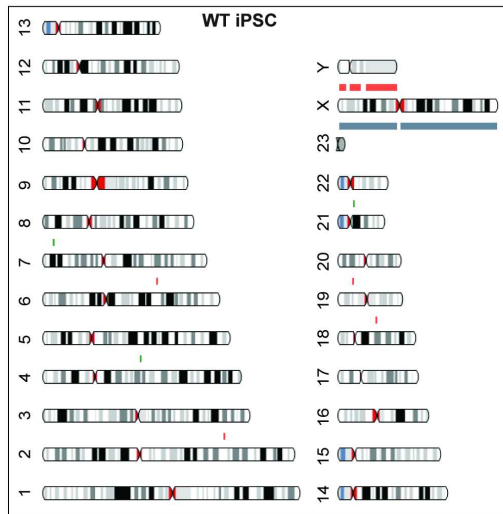
WT
KO allele 1
KO allele 2

PAM
CCACGAGCTGCCGTTTTATGGgt
CCA.....TTTTATGGgt
C.....TGCCGTTTTATGGgt

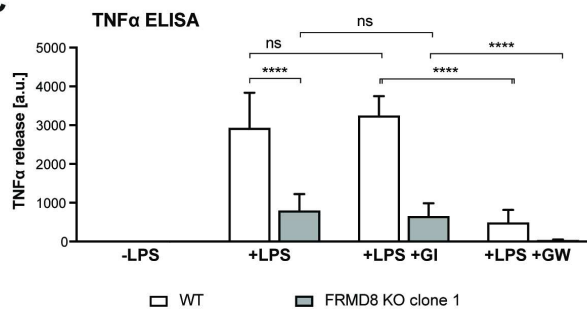
exon 7'intron
7 and 10 nt deletions



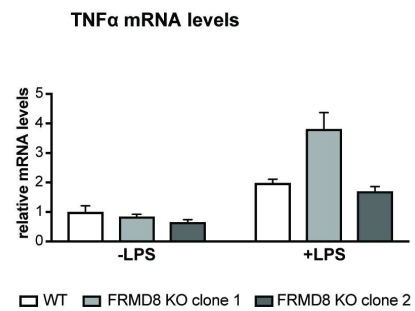
B



C

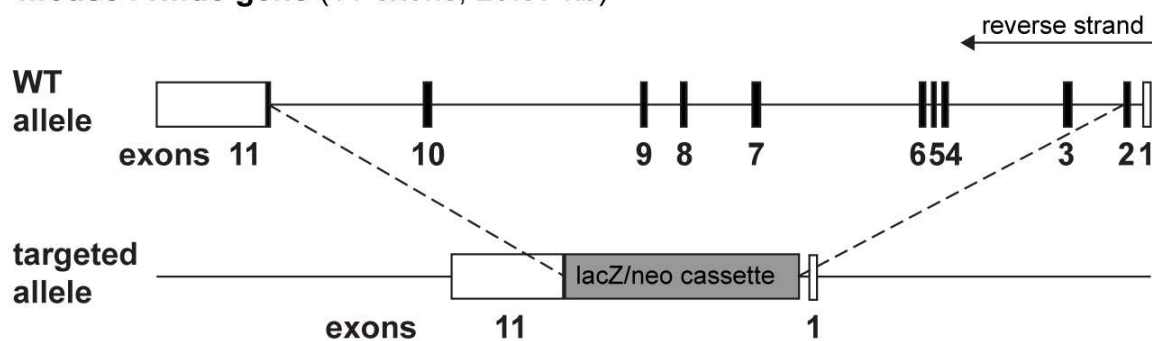


D



A

mouse *Frmd8* gene (11 exons; 25.57 kb)



B

Mouse strain	Breeding	Offspring			
		Total	WT	HET	HOMO
<i>BL6 with neomycin cassette</i>	HET (F) x HET (M)	77	29 (37.66%)	29 (37.66%)	19 (24.68%)
<i>BL6 without cassette</i>	HET (F) x HET (M)	44	12 (27.27%)	18 (40.91%)	14 (31.82%)

C

